Batteries & Supercaps

Review
doi.org/10.1002/batt.202200545

Chemistry Europe
European Chemical Societies Publishing

www.batteries-supercaps.org

Special Collection

Covalent Organic Frameworks as Emerging Battery Materials

Zhiqiang Wang,[a] Jing Hu,[a] and Zhouguang Lu*[a]

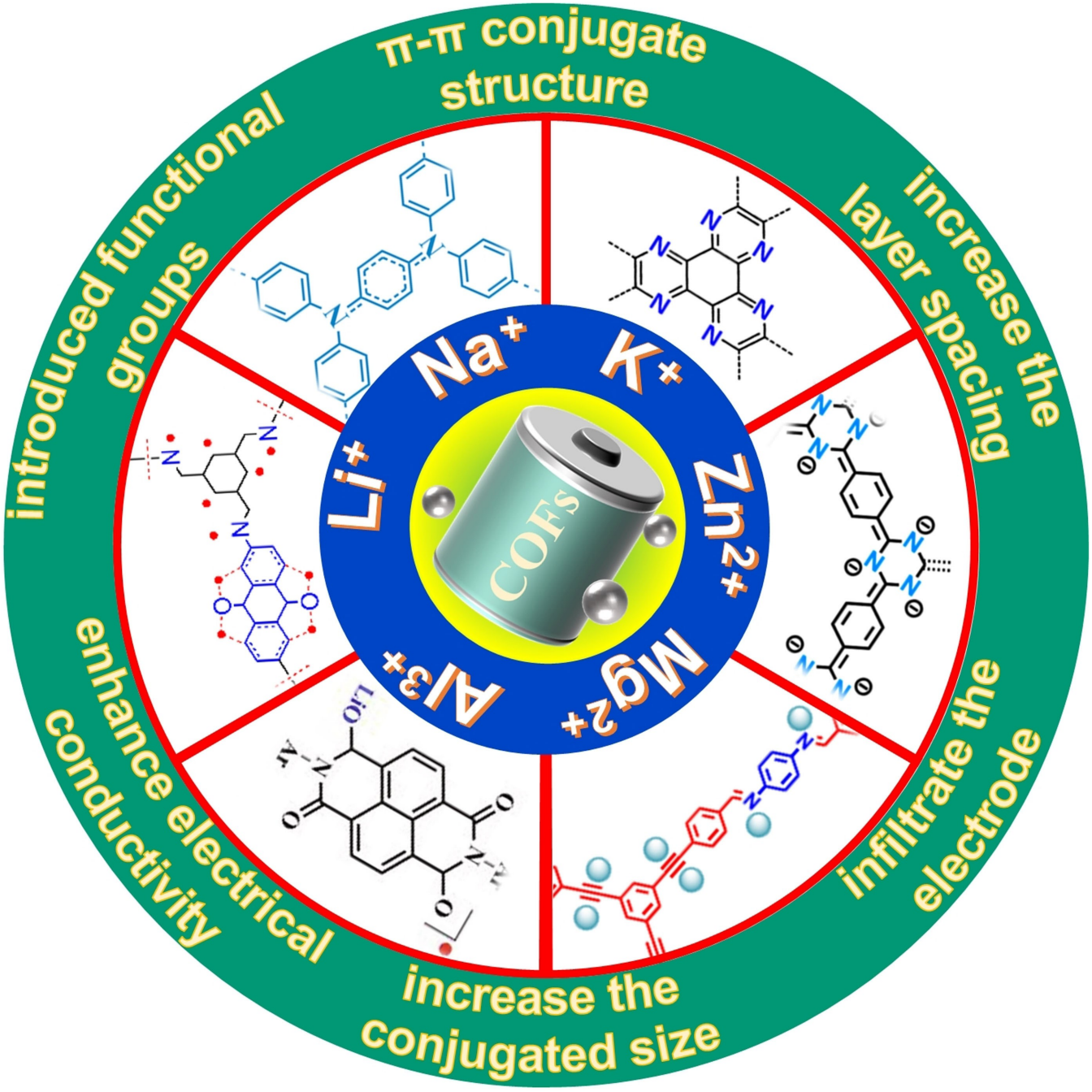

Covalent organic frameworks (COFs) are emerging as promising energy storage materials due to their unique characteristics, such as adjustable thickness, designable topology, superior stability and controllable pore size distribution. Consequently, COFs can provide diversified high-rate carrier transport pathways, and the performance of COFs can be easily improved by adjusting conjugated skeleton types, overlapping p-electron clouds between stacks, and modifying open channels with functional groups. The state-of-the-art COFs electrode materials based on synthetic method and electrochemical performance in recent years are summarized and discussed in this review. The synthesis method, topological structure and application in metal ion (such as Li^+, Na^+, K^+, Zn^{2+}, Mg^{2+}, Al^{3+}, et. al) batteries of COFs electrodes are critically accounted. Finally, we briefly discuss the major challenges in the field that needs to be addressed to pave the way for industrial applications. Although there are still many arduous tasks to be tackled, the burgeoning of COFs-related technologies and applications in batteries provide a ponderable field for commercial process in the short run.

1. Introduction

Metal-ion batteries are currently widely used in various portable electronic devices and are expected to be widely used in electric vehicles and smart grids.[1] The electrode materials of commercial ion batteries are mainly inorganic transition metal oxides and phosphates.[2] However, most of the transition metal resources are non-renewable, and the battery recycling technologies are complicated and expensive. Thus, resource shortage will be the major problem impede the application of metal-ion batteries in the near future.[3] Therefore, developing recyclable electrode materials has stepped into the central and academic frontier in battery field.

COFs, as a burgeoning category of crystalline cellular material connected by covalent bonds with long-range order topology structure, are consisted of pure organic substance based on lightweight elements (C, H, O, N and B).[4] The carbon dioxide produced by COF materials in the process of organic material extraction and preparation, battery assembly and recycling can be absorbed and utilized by plants, reflecting excellent recyclability and renewability.[5] Since the report of COF-1, the research of COF materials has been carried out rapidly and exciting progress has been made worldwide.[6]

COFs are porous organic crystalline materials connected by covalent bonds.[7] In addition, COF electrode materials are hardly to dissolve in electrolytes because of its strong and extended framework than small organic molecules. And compared with other traditional polymers, COF possess unique crystal structure and environmental characteristics are also widely concerned. COFs exhibit abundant synthesis methods and diversified topological structures thanks to the various designability of organic monomers, the order and regularity of crystal materials and the diversity of covalent bond forms.[8] The crystallization, porosity, π-electron conjugation system and π-π stacking between the layers endow COF materials excellent physicochemical properties, especially in electrochemical energy storage.[9] The π-π conjugated structure makes COF materials possess marvelous flexibility, mechanical strength and chemical stability.

The structure and characteristics of COFs are determined by the variation of building blocks with different geometric shapes and sizes.[10] Furthermore, the physical and chemical properties of the COFs can be regulated by carrying a desired functionality on the organic monomers.[11] The unique crystal structure of COFs enables uniform distribution of pores with adjustable pore size, which signifies low-density and high specific surface area, thus facilitating the COFs to sufficient contact with the electrolyte.[12] Moreover, the appropriate structure of COFs can facilitate the electrolyte ions and electrons intercalate and extract during charge and discharge process, resulting in improved rate performance and cycle stability.[13] These attractive inherent characteristics endow COFs with great potential in electrochemical energy storage application.

In recent years, the COFs-based electrode materials with adjustable pore size, topological structure and interlayer spacing have demonstrated infinite possibilities in electrochemical direction. With the upsurge of publications in the field of COF-based metal-ion batteries, a comprehensive review of COF electrodes is needed. In this review, the design principles, synthesis methods and topology of COFs are summarized to facilitate the optimization and application of COFs in rechargeable batteries for the first time. The applications of COFs in rechargeable metal-ion batteries (such as Li^+, Na^+, K^+, Zn^{2+}, Mg^{2+}, Al^{3+}, etc.) are further highlighted. The basic principles and transfer mechanisms of metal ions in COFs are also emphasized. Finally, the development prospect and challenges of COFs in metal-ion batteries are pointed out. The aim of this review is to promote the development of COF materials and enlighten the invention of metal-ion batteries with high performance.

2. Synthesis Strategies and Topological Structure Design of COFs

COFs possess unique crystalline and highly ordered porous structure, and demonstrate abundant and controllable desgin and fabrication routes.[14] The adjustable pore size and functional covalent organic skeleton are the most intriguing characteristic of COFs.[15] Meanwhile, the abundance of select-

[a] Z. Wang, Dr. J. Hu, Prof. Z. Lu
Department of Materials Science and Engineering
Shenzhen Key Laboratory of Interfacial Science and Engineering of Materials
Southern University of Science and Technology
Shenzhen 518055 (China)
E-mail: luzg@sustech.edu.cn

Special Collection An invited contribution to a Special Collection on Organic Batteries

able monomers and synthetic methods form disparate topological structures, which provides more possibilities for the application of COF materials in the electrochemical field.[16] As a common synthetic strategy for COFs, the bottom-up polymerization confers COFs with pre-designable structural characteristics, including the functional groups with uniform distributed.[17] Moreover, the electrochemical reaction platform of the COFs batteries can be regulated by selecting the electron-withdrawing and electron-donating functional groups in the framework, which lays a solid foundation for their practical application.[18] The diffuse capacious π-conjugated framework structures in COFs are able to optimize the battery dynamics and physicochemical stability of electrode materials during charging and discharging process.

2.1. Synthetic reactions and strategies for COFs

The synthesis of conjugated COFs mainly depends on the solvothermal condensation reaction which triggered dynamic covalent bond process to obtain highly crystalline COFs.[19] The water concentration in solvothermal method is controlled by the closed system. Maintaining a steady concentration of water can maximize the formation of reversible covalent bond.[20]

In 2005, Yaghi pioneered the strategy of solvothermal condensation and boric acid coupling reaction to synthesize COF (Figure 1a).[6,19] Mixed organic solvents are usually selected as the reaction medium for COFs synthesis, because they can maintain the steerable diffusion behavior of organic monomer in solution and facilitate the nucleation of COFs.[21] Since then, the solvothermal condensation method has been widely used for the preparation of COFs. Subsequently, a high temperature ion-thermal synthetic strategy was developed by Arne Thomas et al. They applied molten ionic salt ($ZnCl_2$) as catalyst and reaction solvent simultaneously, after programmed gradient temperature rose to 400 °C for 40 h, the covalent triazine framework (CTF-1) (Figure 1b) was successfully synthesized.[22]

The nucleophilic aromatic substitution reactions were also used to synthesize COF materials. Jong-Ho Kim et al. successfully synthesized PTCOF (Figure 1c) by amino coupling reactions between halogen atomic (chlorine) functional groups of 2,6-diaminopyridine and amino functional groups of cyanuric chloride in acetonitrile.[23] The PAE-COF (Figure 1d) was successfully prepared by amino coupling reaction between catechol and ortho-difluoro benzene building blocks.[24] In general, most COFs are prepared by condensation of two or more building blocks with different reaction sites. With the continuous research and development, coupling reactions has become the mainstream reactions applied for synthesis of COFs, which include boric acid coupling, cyan group coupling reaction, amino coupling reaction and other coupling reactions (Figure 1).

In order to optimize the synthesis conditions of COFs and reduce the reaction time and cost, scientists have been constantly seeking for faster and more convenient synthesis methods. The synthesis strategies based on ultrasonic, hydrothermal, microwave and mechanochemical synthesis methods have been applied to synthesize COFs.[25] Byeong-Su Kim et al. first successfully prepared highly crystalline polyimide-based COF materials (PICs) by hydrothermal polymerization strategy. Aromatic diamines of different sizes reacted with triphenylene-2,3,6,7,10,11-hexacarboxylic acid to synthesize PICs with different crystallinities and pore dimensions.[26] Most importantly, the crystallinity of COF synthesized by hydrothermal method is higher than that of COF prepared by traditional solvothermal method. Using magnesium metal powders as catalyst, Sheng Dai et al. successful synthesized phthalocyanines-functionalized covalent organic frameworks (Pc-CPNs) from ortho-positioned dicyano aromatic nitrile building blocks by short time ball-milling method.[27] The Pc-CPNs synthesized by mechanochemistry-driven strategy showed distinguished mechanical and electrochemical properties. By introduced p-toluene sulfonic acid as a solid acid catalyst during the polymerization reaction of cyan group units, crystalline and porous triazine-based COFs

Wang Zhiqiang is a PhD candidate at the Department of Materials Science and Engineering, Southern University of Science and Technology, China under the supervision of Prof. Zhouguang Lu. His research focuses on organic energy storage materials design and control for metal-ion batteries applications.

Dr. Jing Hu is currently senior research fellow in Southern University of Science and Technology. She obtained her BE (2010) and MSc (2013) in Applied Chemistry from the Central South University (CSU) in China and PhD (2020) from The Hong Kong Polytechnic University in Hong Kong. Her research is focused on electrochemical energy storage and conversion, with an emphasis on the development of lithium sulfur batteries, lithium-ion batteries.

Dr. Zhouguang Lu obtained his Ph.D. from the City University of Hong Kong in 2009. He is now full professor at the Department of Materials Science and Engineering, Southern University of Science and Technology. His research interests include the design and synthesis of nanostructures and their applications in energy storage and conversion.

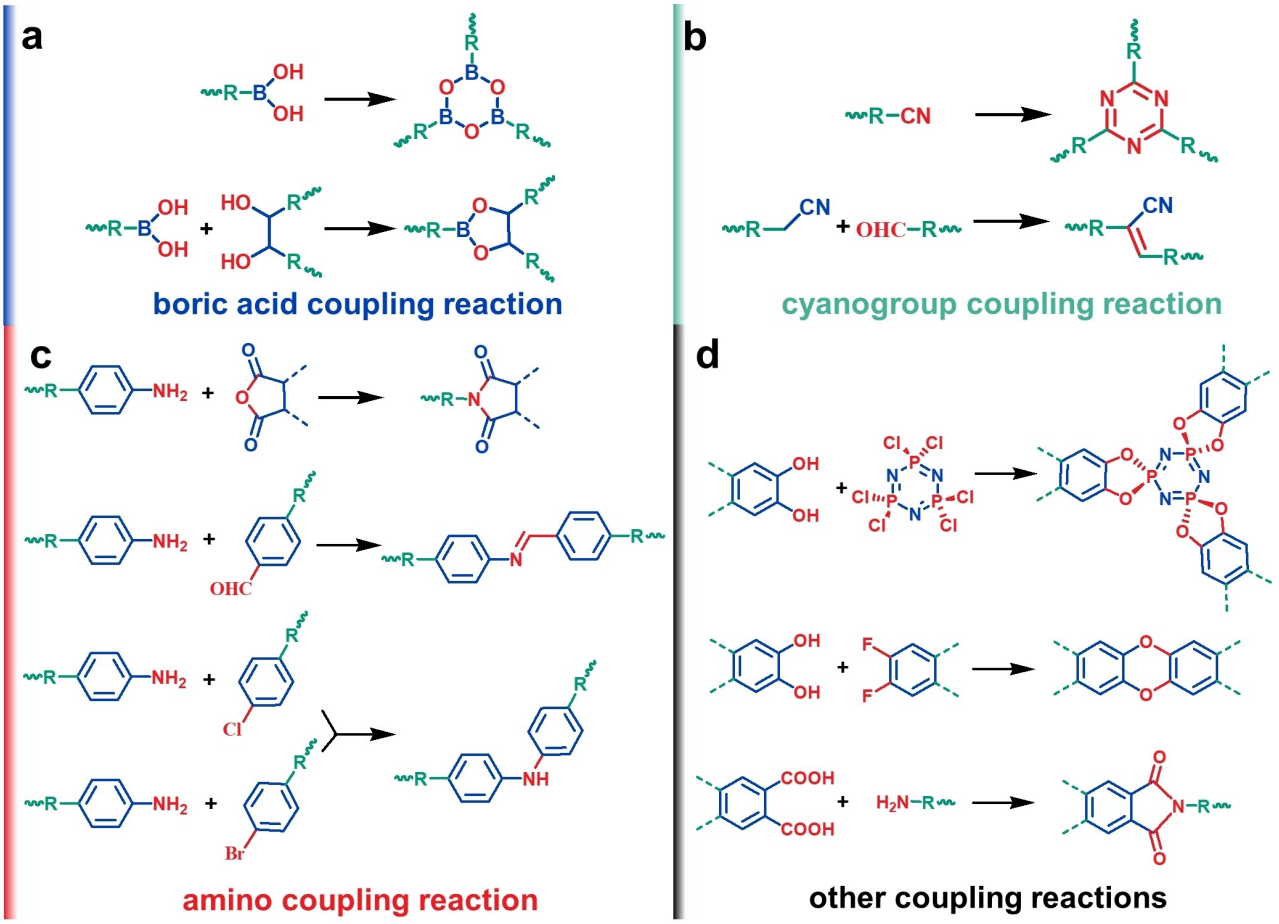

Figure 1. The schematic diagram of synthetic reactions and strategies for COFs.

can be synthesized within a few minutes.[28] The assistance of microwave and ultrasonic technology also accelerates the reaction process and greatly shorten the reaction time.[29]

The current COFs preparation strategies have high yield and purity, and are widely used for 2D and 3D-COFs preparation. Stable reaction environment is conducive to orderly extension of COF materials with higher degree of polymerization, and suitable synthesis methods can be selected according to specific experimental conditions. Solvothermal method exhibits excellent general applicability, but the synthesis process takes the longest reaction time and generally higher temperature (120 °C for 3 d). Because of the simple operation, low cost, easy control process, the solvothermal method is widely used for COFs synthesis. The synthesis temperature of ionic thermal method is the highest among the aforementioned synthetic strategies and the synthesis time is longer (400 °C for 40 h). Microwave-assisted reaction method shows shorter reaction time and lower temperature (100 °C for 1 h). The catalytic-mechanical ball-milling method takes less reaction time, but the operation requires more stricter safety and professional operation. More and more methods for COF synthesis have been developed, and the synthesis methodology based on COF materials has been continuously developed and expanded.

2.2. Topological structures of COFs

To prepare long-range ordered and highly crystalline COFs, the reactive groups can cause dynamic covalent bond formation and must be contained in the building unit structure. And the bonding direction of the block must be discrete and rigid in conformation.[30] The discrete bonding direction and rigid conformation of the blocks enable to design COFs based on topological theory. The two-dimensional (2D) or three-dimensional (3D) structural COFs can be constructed with different topologies by flexible selecting building units that differ in key factors such as geometry, symmetry, length, connectivity and dihedral angles.[31] For 2D COFs, precursors are connected by covalent bonds to form layered structures in the plane, and the conjugate system is formed between layers through π-π interaction. At the same time, one-dimensional channels are also formed, whose inner diameter and shape are closely related to the stacking mode between layers.[32] For 3D COFs, building units infinitely extended through covalent bonds to form a cage with regular and periodic structure. Compared with 2D-COFs, 3D COFs form larger cavities in the process of 3D space extension, in which organic units continue to react in the cavities and grow outwards. Therefore, multiple interspersed

structures are often obtained in the resulting products for 3D-COFs.[33]

2D-COFs possess covalent organic skeleton that extends sequentially alongprep the two-dimensional plane.[34] The diameter and shape of channels in 2D-COFs can be designed by selecting building blocks with different size, geometry and symmetry combinations (Figure 2). In general, rigid hexavalent (C_6), tetravalent (C_4), trivalent (C_3) and divalent (C_2) ligands are selected as 2D-COFs component units.[35] 2D-COFs are generally obtained by condenzation reaction with selecting a knot and a linker.[36] The common combinations to build 2D-COFs are [C_2+C_2], [C_3+C_2], [C_3+C_3], [C_4+C_2], [C_4+C_4], [C_6+C_2] and [C_6+C_3] (Figure 2). The reaction between two divalent [C_2+C_2], trivalent and divalent [C_3+C_2] or two trivalent ligands [C_3+C_3] will produce hexagonal **hcb** topology (Figure 2a–c). The combination of tetravalent and divalent [C_4+C_2] or two tetravalent ligands [C_4+C_4] will lead the form of **sql** topology (Figure 2d, e and h). Based on the principles of topology, the combinations of tetravalent and divalent ligands [C_4+C_2] with C_2 axisymmetric structure can result in single pore **sql** or dual pore **kgm** topologies (Figure 2f, g). The **hxl** topology structure can be constructed by reaction of hexavalent and divalent ligands [C_6+C_2] (Figure 2i). The hexavalent linker reacts with trivalent ligands [C_6+C_3] to form **kgd** topology structure (Figure 2j).[37] The combination of COFs with one knot and two or more linkers has been confirmed based on the general topology.[38] The rigidity of the blocks and the dispersion of the bonding directions make 2D-COFs highly flexible in the design of molecular structures.

Compared to the 2D-COF materials that have emerged in an endless stream, the development of 3D COF is lagged behind, mainly because of the finite amount units used to construct 3D structure and complex structure analysis. In 2007, the Yaghi group reported four 3D-COFs for the first time.[39] The key to design the 3D-COFs with **ctn** and **bor** topological structure is the selection of tetrahedral building blocks with **Td** symmetry (tetra(4-dihydroxyborylphenyl) silane) combined with C_3 units.

In 2018, Wang et al. achieved large size single crystals of 3D-COF based on imine bonds. The high quality of the crystals made the COFs amenable to single-crystal X-ray characterization for the first time.[40] The formation of 3D-COFs usually requires participation of at least one 3D molecule. At present, the monomers used to construct 3D-COFs are mainly the building blocks of symmetry in stereo, such as regular tetrahedron, triangular bipyramid, triangular prismatic structures and so on.[41] The differences of bond directions, linker lengths and spatial configurations can form secondary channels, tertiary porous and 3D stereoscopic COF materials.

The rigid element of the structure is the basis of COFs as electrode material, which is the key to maintain the rechargeable stability of electrochemical performance. The crystallization of COFs may promote the uniform distribution of the spatial topology, and the uniform porous channels regularly distribution are going to enhance the mass transfer dynamics,

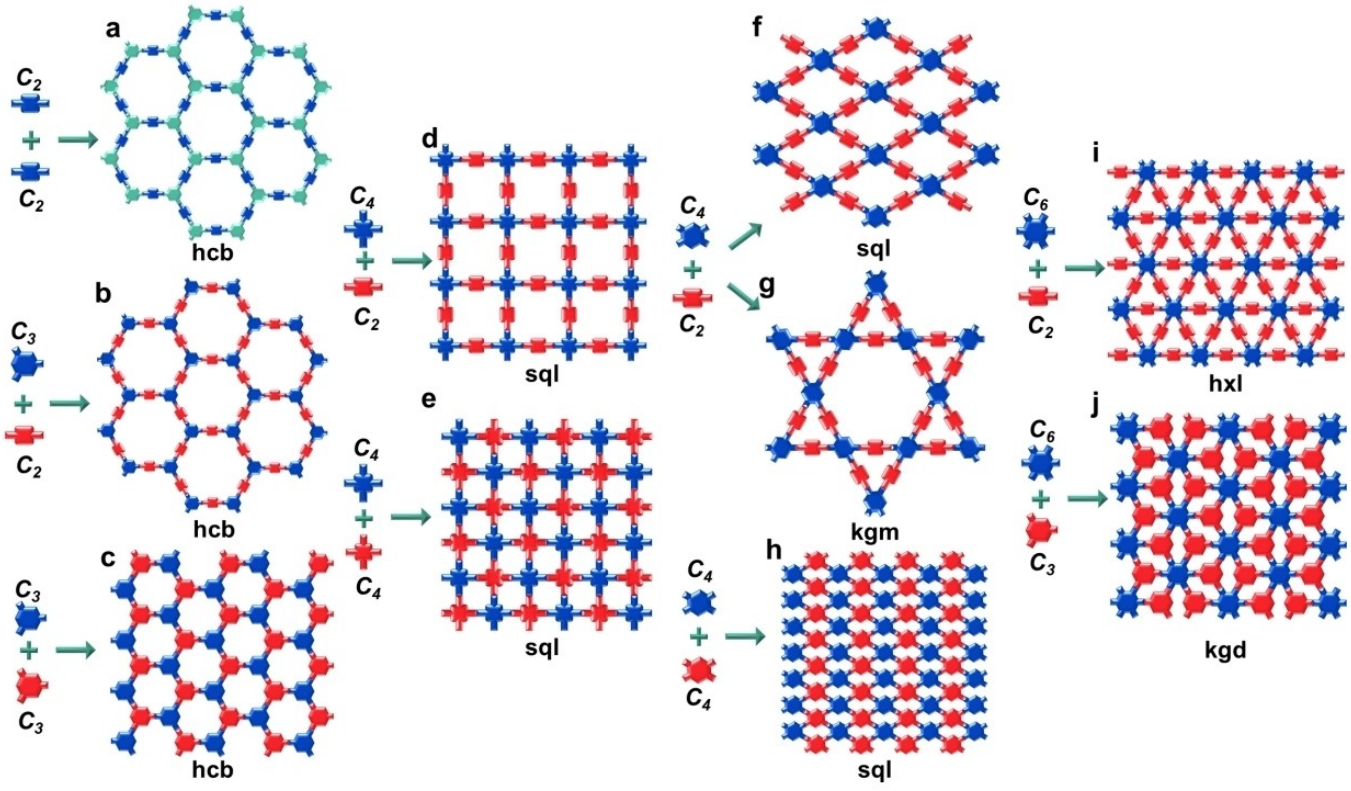

Figure 2. The topological structures of monomer symmetry and lattice for 2D-COFs (C_n: there are *n* reactive terminals in the building units).

improve the transmission efficiency, and thus increase the rate performance. The large surface area of the COFs may provide more exposed active sites in contact with the electrolyte, thereby enhancing coulombic efficiency during the rechargeable process. The large π-conjugate structure enables the COFs possess excellent electrical conductivity. In addition, the electrochemical reaction platform of COFs can be adjusted by introducing functional group modification.

3. COFs for Rechargeable Metal-Ion Batteries

Covalent organic frameworks (COFs) exhibit the preponderance of limited solubility in electrolytes, long-range order pore structure, distinguished chemical stability, remarkable thermostability, excellent mechanical strength and high rechargeable capacity.[42] Furthermore, the transition of COFs crystalline structure is remained stable during the adsorption/desorption process of metal ions, and the reaction kinetics responds quickly. Moreover, the rapid insertion and removal of metal ions does not cause the structural degradation of the electrode, which ensures the cycling performance and rate performance of metal-ion batteries. Benefited from these advantages, COFs present a broad application prospect in metal-ion battery (e.g., Li^+, Na^+, K^+, Zn^{2+}, Mg^{2+}, Al^{3+}, etc.) electrode materials

The electrochemical performance is closely related to active sites in COFs. The reversible capacity of metal-ion batteries generally depends on the stable reversible redox reaction at the active site, which combines positive or negative charges through the redox state during the charging and discharging process. Common building block structures with active site are summarized in Figure 3, and the active sites in the units were highlighted in red. The COF electrodes are classified into n-type, p-type and bipolar types according to the transformation behavior of the free radical state during the charging and discharging process.[42c] The reduced n-type organic active sites can generate anion radicals that can bind to metal ions or other cations. The common n-type active sites in COFs electrode materials are oxygen anion radical of carbonyl groups (C–O^-) and nitrogen anion radical of imine groups (C–N^-). The p-type organic active sites lost electrons and become cation radicals that combine with anions in the electrolyte, during the charging process. The typical p-type active sites in COFs are nitrogen cation radicals of nitronyl nitroxides (N–O^+), sulfur cation radicals of organic sulfide structure (C–S^+) and nitrogen cation radicals of triphenylamine units (N–C^+). The bipolar active sites can be reduced or oxidized within a specific voltage range during rechargeable process. The polyaniline units (C–N) is a typical bipolar active site, in addition to triazine ring (C_3N_3) and nitro (N–$O^•$) also exhibit bipolar radical properties.[43]

In order to prepare COF materials with high capacity and stability, it is necessary to select suitable building units possess active sites. The design and synthesis of single-active site, dual-active site and multi-active sites COFs were carried out by the predesigned precursors. The process of metal ions and anion ions insertion/extraction mainly depends on the redox process of the active site on the COFs electrode materials. It should be noted that the number of carbonyl groups does not directly determine the specific capacity of the COFs electrode. As shown in Figure 3, four carbonyl groups within a conjugate unit are usually bound to two metal ions. However, the carbonyl group can conjugate with the benzene rings on the

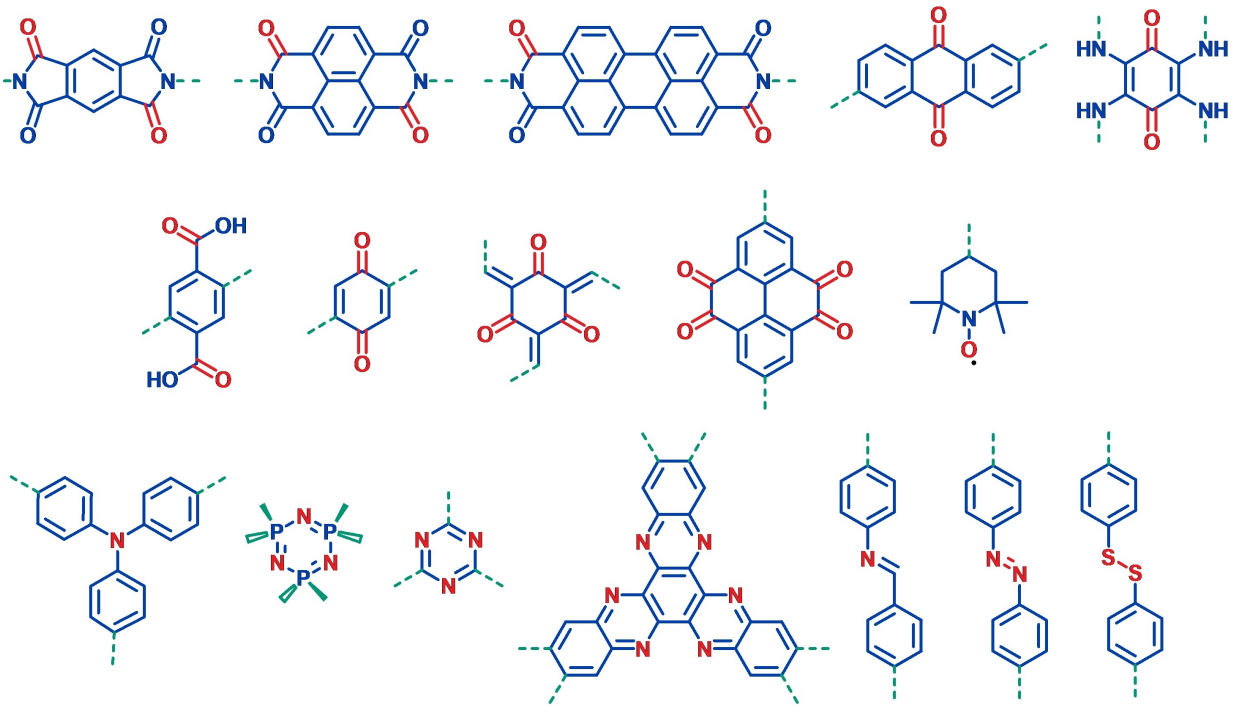

Figure 3. Summary of redox active units in COFs.

skeleton to improve the utilization ratio, so that truxenone units can combine with 6 Li^+ ions.[44] In addition, at low current densities, the C=C functional group generates super-lithification due to the conjugation effect of the electrode structure to form the active site of the C6–M6 (Li^+ or Na^+) structure, such as anhydride-based COF and carbonyl-based COF materials.[41b] Obviously, the chemical environment and steric hindrance of the local molecular structure also determine the utilization of the active sites. Therefore, the specific capacity of COFs electrode materials depends not only on the number of active sites, but also on the local molecular structure and topological structure, which should be taken into account when designing novel COFs electrode materials.

3.1. COFs for lithium-ion battery

In the field of lithium-ion batteries (LIBs), the π-conjugate system, open channels and porous structure of COFs are favorable for charge exchange and Li-ion transportation. There are many active sites in COFs, which are uniformly distributed and can be embedded with lithium ions. The excellent physicochemical stability of COFs ensures the excellent cycling stability of LIBs. Therefore, COFs can be used as potential lithium ion electrode materials. At the same time, how to improve the electrochemical performance of COFs electrode materials has become a new challenge. In order to maintain the stability of free radical intermediates cycling in the redox process of organic active units. The polyimide-based COF materials (Figure 4a) combined with perylene (Pe-PICOF), naphthalene (Na-PICOF) and benzene (Be-PICOF) building blocks were successful prepared by our group.[45] The spin electron densities, charge transport capacity and molecular orbital energy of reaction substrates in PICOFs were regulated by adjusting the size of conjugated system to ameliorate the stability and reactivity of free radicals. The PICOFs cathode electrode materials displayed obvious discharge plateaus of 2.47, 2.42 and 2.01 V for Pe-PICOF, Na-PICOF and Be-PICOF at 50 mA g^{-1}, respectively (Figure 4b). The initial discharge capacities (Figure 4c and Table 1) were 91, 102 and 114 mA g^{-1} for Pe-PICOF, Na-PICOF and Be-PICOF at 50 mA g^{-1}, respectively. And after 100 cycles, Pe-PICOF and Na-PICOF exhibited excellent capacity retentions (Figure 4d) for 96% and 92%, respectively. At the current density of 1000 mA g^{-1}, Pe-PICOF and Na-PICOF showed capacity retentions (Figure 4e) of 81% and 76% after 10,000 cycles, respectively.

The redox mechanism was speculated by ex-situ electron paramagnetic resonance (EPR) spectra and DFT calculation as shown in Figure 4(f, g). The imide radical intermediate (Figure 4f) translated to enol lithium salt or imide substrates by gaining or losing of Li^+ and electron. The intensity of radical signal increased and decreased in EPR spectra (Figure 4g) obviously accompanied by the production and disappearance of free radicals. Combined with the theoretical DFT calculation, the results indicate that the COFs electrode with larger imine conjugated unit had better free radical electron delocalization effect and electrochemical stability. In addition to regulating free radical stability, the conductivity of COFs also has a great influence on the properties of electrode materials. Hye Ryung Byon et al. successfully synthesized a series of azo-linked COFs based on the thiazole group, which exhibited outstanding conductivity.[46] Furthermore, the azo functional group further demonstrated rapid two-electron transfer in Azo1 COFs. TAPB-NDI COF confirmed the macropores structure in the reported structure contributes to efficient transport of Li^+ ion transport.[47] Thus, the design of COFs conjugated structure is the key to keep the redox reaction stable during charging and discharging process.

Subsequently, a novel polyimide COF based on N,N,N,N-tetraphenylphenylenediamine (TPPDA) monomers was synthesized, which processed dual pore **kgm** topologies (Figure 5a).[48] The quite high voltage platform of TPPDA-PICOF electrode was 3.6 V during discharge process. During the discharge process, the EPR (Figure 5b) signal intensity of the TPPDA electrode increased from 4.1 V to 3.8 V, then decreased until discharged to 2.6 V, which confirmed the formation and disappearance of TPPDA free radical cations during discharge process. Combined with DFT calculation and experimental data, we speculated the active site in TPPDA-PICOF was the nitrogen atom in TPPDA. As shown in Figure 5(c), during the discharge process, TPPDA divalent cation lost a PF_6^- anion and accepted one electron, then the TPPDA divalent radical cation translated to a TPPDA cation. subsequently, TPPDA radical cation continued to lose a PF_6^- anion and accept one electron to become TPPDA original state.

Yongsheng Chen et al. synthesize the PA-TA COF (Figure 5d) based on piperazine-terephthalaldehyde.[49] The PA-TA COF possessed ultra-large interlayer distance up to 6.2 Å and demonstrated excellent cycling and rate performance. In addition, the capacity of PA-TA COF retained 543 mAh g^{-1} at 1.0 A g^{-1} after 400 cycles.

Qichun Zhang et al. reported a dual active centers (N=N and C=N) TA COF (Figure 6a) anode electrode materials. by fabricating with 1,3,5-triformylbenzene (Tb) and 4,4′-diazoanilidine (Azo).[50] The TA COF maintained a reversible capacity for 227 mAh g^{-1} at a high current density of 5 A g^{-1} after 2000 cycles (Figure 6b). They revealed the structural evolution of TA COF by DFT calculation (Figure 6c). The N=N units was first lithiated, because the electrostatic potential of the C=N group was higher than that of N=N group. For discharge process, 12 Li^+ ions were firstly received by the N=N units accompanied with forming the COF-12Li structure, then 18 Li^+ ions reacted with the C=N units to form the COF-30Li structure. A similar Li30-accommodating structure had been previously reported, in which TP-OH-COF was prepared by 2,5-diaminohydroquinone dihydrochloride and triformylpholoroglucinol.[51] The high specific capacity of Li30-TP-OH-COF was achieved by carbonyl and hydroxyl active sites.

Hui Dou's group synthesized another double active site (C=O and C=N units) DAAQ-COF (Figure 7a) based on the precursor of 1,3,5-benzenetricarboxaldehyde (Tb) and 2,6-diaminoanthraquinone (DAAQ) by condensation reaction.[52] The addition of introduced functional groups with active sites can improve the theoretical capacity of DAAQ in Li-ion

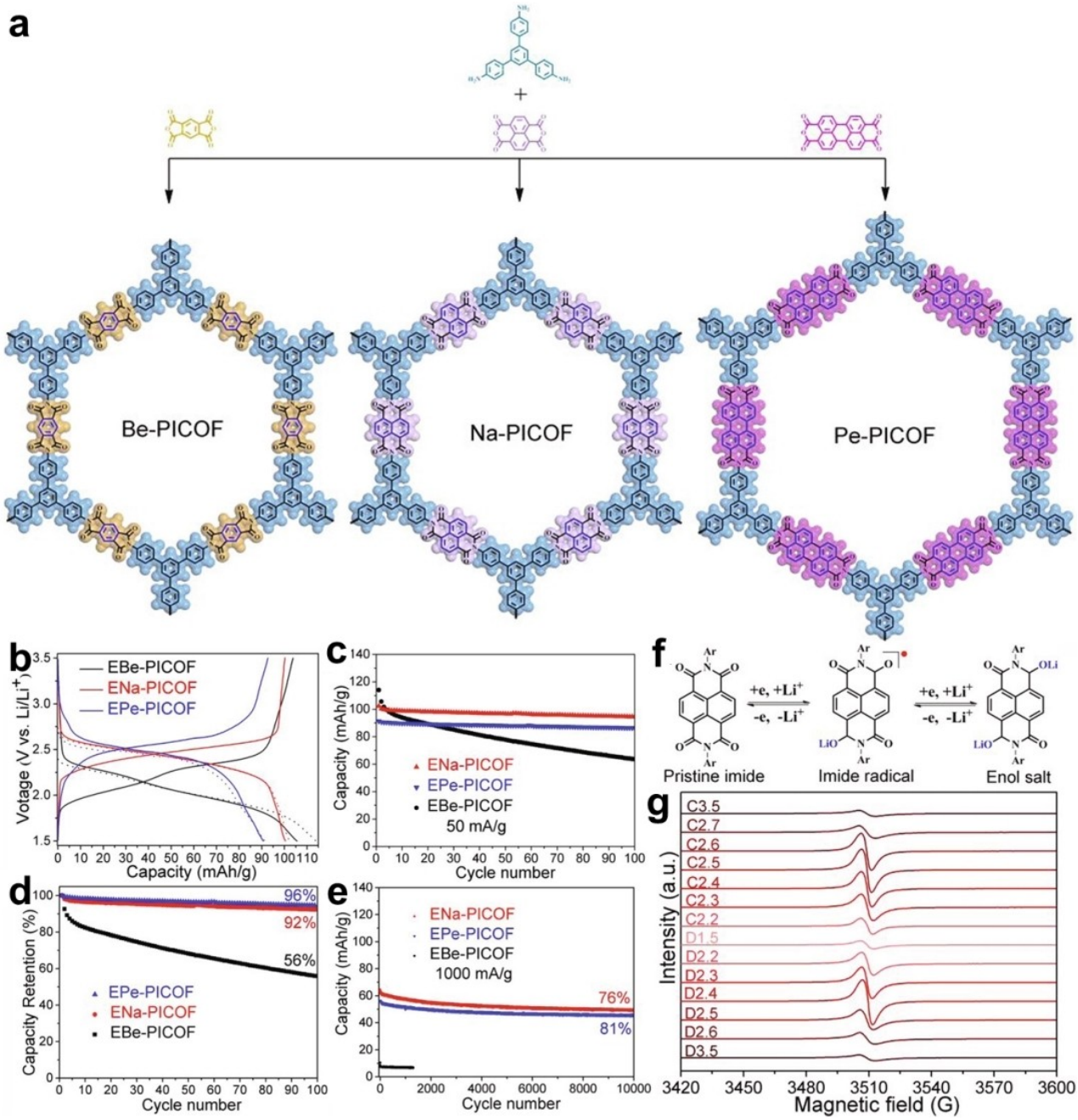

Figure 4. a) Chemical structures of PICOFs. b) Electrochemical performance of PICOFs. c) Cycling performance at 50 mA g^{-1}. d) Capacity retention at 50 mA g^{-1}. e) Cycling performance at 1000 mA g^{-1}. f) Representative redox mechanism. g) Ex-situ EPR spectra of Na-PICOF. Reproduced with permission from Ref. [45]. Copyright (2022) Elsevier.

batteries. DAAQ-COF showed excellent high capacity and long-term cycling performance at 1 A g^{-1} (Figure 7b). The discharge capacity of DAAQCOF first suffered a capacity decay before 50th cycles, and then increased to 787 mAh g^{-1} after 500th cycles. The capacity decreasing during the first 50 cycles might be related to irreversible side reaction and the formation of solid electrolyte interface (SEI). The capacity increasing after 50th cycle was connected with the gradually activation of C=O and C=N active sites. Furthermore, aromatic bonds (C–C) also participated in the 10 Li^+ lithiation process (Figure 7c) and contributed to the outstanding capacity.

The TP-DA-COF was synthesized by pyrazine-2,5-diamine (DA) and 1,3,5-triformylpholoroglucinol (Tp).[53] In order to solve the slightly poor conductivity and sluggish lithium-ion diffusion kinetics of TP-DA-COF, carbon nanotubes (CNTs) were used as a carrier and enshrouded by TP-DA-COF by in-situ reaction. COF@CNT-2 (36 wt% CNT) possessed outstanding electrochemical stability and reversible capacity. In addition, TPB-DMTP-COF was used as a desirable filler in ionic gel electrolyte (IGE), which significantly enhanced the electrical conductivity of the polymeric ionic liquid/ionic liquid (PIL/IL) system.[54]

Table 1. Summary of the application of COFs in metal-ion batteries.

COFs	Modification strategy	Applications	Electrolyte [v/v]	Capacity [mAh g^{-1} at A g^{-1}]	Capacity retention [%/mAh g^{-1} at A g^{-1} (number of cycles)]	Ref.
Be-PICOF	conjugated unit size	cathode	1 M LiTFSI (DME:DOL = 1:1)	114 at 0.05	56% at 0.05 (100)	[45]
Na-PICOF	conjugated unit size	cathode	1 M LiTFSI (DME:DOL = 1:1)	102 at 0.05	76% at 1 (10000)	[45]
Pe-PICOF	conjugated unit size	cathode	1 M LiTFSI (DME:DOL = 1:1)	91 at 0.05	81% at 1 (10000)	[45]
AZO-1 COF	azo-linked	cathode	1 M LiTFSI (DME:DOL = 1:1)	140 at 0.06	100% at 4.8 (5000)	[46]
AZO-2 COF	azo-linked	cathode	1 M LiTFSI (DME:DOL = 1:1)	60 at 0.12	29% at 1.2 (100)	[46]
AZO-3 COF	azo-linked	cathode	1 M LiTFSI (DME:DOL = 1:1)	40 at 0.12	60% at 1.2 (100)	[46]
TAPB-NDI COF	large pore distribution	cathode	0.7 M $LiPF_6$ (EC:PC:DMC = 1:1:3)	33 at 0.03	100% at 0.2 (400)	[47]
TPPDA-PICOF	high discharge voltage	cathode	1 M $LiPF_6$ (EC:DEC:EMC = 1:1:1)	40 at 0.2	98% at 0.2 (200)	[48]
PA-TA COF	ultra-large interlayer distance	anode	1 M $LiPF_6$ (EC:EMC = 3:7)	556 at 0.25	100% at 1 (200)	[49]
TA-COF	dual active centers	anode	1 M LiTFSI (DME:DOL = 1:1)	433 at 0.1	81% at 5 (200)	[50]
TP-OH-COF	Li30-accommodating structure	anode	1 M $LiPF_6$ (EC:DEC = 1:1)	764 at 0.1	63% at 5 (8000)	[51]
DAAQ-COF	dual active centers	anode	1 M $LiPF_6$ (EC:DEC:EMC = 1:1:1)	787 at 1	46% at 5 (8000)	[52]
TP-DA-COF	condensation reaction	anode	1 M $LiPF_6$ (EC:DEC = 1:1)	189 at 0.1	—	[53]
COF@CNT-1	COF@CNT	anode	1 M $LiPF_6$ (EC:DEC = 1:1)	378 at 0.1	—	[53]
COF@CNT-2	COF@CNT	anode	1 M $LiPF_6$ (EC:DEC = 1:1)	570 at 0.1	100% at 1 (2000)	[53]
DAAQ-TFP-COF	condensation reaction	anode	2 M LiCl (Ph = 11.5 LiOH)	132 at 0.5	87% at 1 (1000)	[74]
NA-NiPc COF	phthalocyanine-based	anode	1 M $LiPF_6$ (EC:DEC:DMC = 1:1:1)	805 at 0.05	127% at 0.2 (700)	[78]
PPDA-NiPc COF	phthalocyanine-based	anode	1 M $LiPF_6$ (EC:DEC:DMC = 1:1:1)	924 at 0.05	142% at 0.2 (700)	[78]
DAB-NiPc COF	phthalocyanine-based	anode	1 M $LiPF_6$ (EC:DEC:DMC = 1:1:1)	1068 at 0.05	81% at 0.2 (700)	[78]
CTFs-1-400	triazine based	anode	1 M $LiPF_6$ (EC:DEC = 1:1)	1363 at 0.1	100% at 1 (1000)	[21c]
CTFs-1-500	triazine based	anode	1 M $LiPF_6$ (EC:DEC = 1:1)	929 at 0.1	85% at 1 (1000)	[21c]
HAT-CQP	pyrazine-like C=N	anode	1 M LiTFSI + 5% $LiNO_3$ (DME:DOL = 1:1)	844 at 0.1	82% at 0.8 (500)	[79]
Tp–Ta-COF	dual active centers	anode	1 M $LiPF_6$ (EC:DEC = 1:1)	735 at 0.2	82% at 0.8 (800)	[80]
Tf–Ta-COF	triazine based	anode	1 M $LiPF_6$ (EC:DEC = 1:1)	502 at 0.2	82% at 0.8 (500)	[80]
Tp–Tb-COF	condensation reaction	anode	1 M $LiPF_6$ (EC:DEC = 1:1)	511 at 0.2	82% at 0.8 (500)	[80]
DCB-COF-450	melting method	anode	1 M LiTFSI + 5% $LiNO_3$ (DME:DOL = 1:1)	630 at 0.1	65% at 0.8 (550)	[75]
DCB-COF-500	melting method	anode	1 M LiTFSI + 5% $LiNO_3$ (DME:DOL = 1:1)	350 at 0.1	–	[75]
TP-TA COF	bipolar-type	cathode	1 M $LiPF_6$ (EC:EMC = 3:7)	207 at 0.2	93% at 5 (1500)	[81]
TP-COF	dual active centers	cathode	1 M LiTFSI (DME:DOL = 1:1)	25 at 0.2	–	[82]
E-TP-COF	dual active centers	cathode	1 M LiTFSI (DME:DOL = 1:1)	110 at 0.2	87% at 0.2 (500)	[82]
PTDCOF	piperazine-based	anode	1 M $LiPF_6$ (EC:DEC:DMC = 1:1:1)	1184 at 0.1	105% at 5 (5000)	[83]
HAB-COF	imine groups	anode	1 M $LiPF_6$ (EC:DEC:DMC = 1:1:1)	351 at 0.1	1225 mAh g^{-1} at 1 (1100)	[84]
Azo-CTF	azo-linked	cathode	1 M LiTFSI (DME:DOL = 1:1)	205 at 0.1	89% at 4 (5000)	[85]
HATN-HHTP	pyrazine sites	cathode	1 M LiTFSI (DME:DOL = 1:1)	125 at 0.05	–	[76]
HATN-HHTP@CNT	growth on CNT	cathode	1 M LiTFSI (DME:DOL = 1:1)	230 at 0.05	100% at 0.5 (6900)	[76]
HATN-HHTP@CNT	growth on CNT	cathode	1 M $NaPF_6$ (DME)	225 at 0.05	100% at 1 (6200)	[76]
Aza-COF	aza-based	cathode	1 M $NaPF_6$ (DEGDME)	363 at 0.6	87% at 3 (500)	[55]
COIHP-1	hexachlorophosphazene-linked	anode	1 M $NaClO_4$ (EC:DEC = 1:1)	310 at 0.035	87% at 0.035 (500)	[56]
NA-NiPc COF	phthalocyanine-based	anode	1 M $NaClO_4$ (EC:DEC = 1:1)	235 at 0.05	94% at 0.2 (900)	[78]
PPDA-NiPc COF	phthalocyanine-based	anode	1 M $NaClO_4$ (EC:DEC = 1:1)	176 at 0.05	93% at 0.2 (900)	[78]
DAB-NiPc COF	phthalocyanine-based	anode	1 M $NaClO_4$ (EC:DEC = 1:1)	103 at 0.05	86% at 0.2 (900)	[78]
TAEB-COF	alkynyl-based	anode	2.76 M KFSI (DME:TTE = 2:1)	505 at 0.05	50% at 0.05 (300)	[57]
TAPB-COF	condensation reaction	anode	2.76 M KFSI (DME:TTE = 2:1)	318 at 0.05	–	[57]
DBA-COF 3	alkynyl-based	anode	2.76 M KFSI (DME:TTE = 2:1)	13 at 0.05	24% at 0.05 (300)	[57]
PI-NTCDA@CNT	growth on CNT	anode	0.8 M KPF_6 (EC:DEC = 1:1)	135 at 0.1	99.6% at 0.1 (1000)	[58a]
PI-NTCDA-CNT	directly physical mixing	anode	0.8 M KPF_6 (EC:DEC = 1:1)	85 at 0.1	–	[58a]
COF-10	condensation reaction	anode	1.0 M KFSI (EC:DEC = 1:1)	130 at 0.1	57 mAh g^{-1} at 0.1 (500)	[58b]
COF-10@CNT	growth on CNT	anode	1.0 M KFSI (EC:DEC = 1:1)	348 at 0.1	161 mAh g^{-1} at 1 (4000)	[58b]
P-COF	condensation reaction	anode	0.8 M KPF_6 (EC:DEC = 1:1)	276 at 0.05	–	[59]
P-COF@SWCNT	growth on CNT	anode	0.8 M KPF_6 (EC:DEC = 1:1)	438 at 0.05	56% at 0.7 (1400)	[59]
DAAQ-COF	condensation reaction	cathode	1.0 M KFSI (EC:DEC = 1:1)	124 at 0.1	–	[86]
DAAQ-COF@CNT	growth on CNT	cathode	1.0 M KFSI (EC:DEC = 1:1)	157 at 0.1	77% at 0.5 (500)	[86]
COF	solvothermal reaction	anode	1.0 M KFSI (EC:DEC = 1:1)	280 at 0.1	106 mAh g^{-1} at 0.1 (400)	[87]
COF-Co	cobalt acetate	anode	1.0 M KFSI (EC:DEC = 1:1)	987 at 0.1	371 mAh g^{-1} at 0.1 (400)	[87]
HATN-HHTP@CNT	growth on CNT	cathode	1.0 M KFSI (EC:DEC = 1:1)	218 at 0.05	86.5% at 0.5 (2400)	[76]
HqTp-COF	direct zinc storage	cathode	3 M $ZnSO_4$ (H_2O)	276 at 0.125	98% at 3.75 (1000)	[63]
PA-COF	phenanthroline unit	cathode	2 M $ZnSO_4$ (H_2O)	247 at 0.1	62% at 1(10 000)	[64]
HAQ-COF	quinone groups	cathode	2 M $ZnSO_4$ (H_2O)	344 at 0.1	85% at 5 (10 000)	[65]

Table 1. continued

COFs	Modification strategy	Applications	Electrolyte [v/v]	Capacity [mAh g^{-1} at A g^{-1}]	Capacity retention [%/mAh g^{-1} at A g^{-1} (number of cycles)]	Ref.
PI-COF	direct zinc storage	anode	2 M $ZnSO_4$ (H_2O)	92 at 0.7	85% at 10 mV s^{-1} (4000)	[66]
BT-PTO COF	quinone groups	cathode	3 M $Zn(CF_3SO_3)_2$ (H_2O)	221 at 1	98% at 5 (10 000)	[67]
Tp-PTO-COF	quinone groups	cathode	2 M $ZnSO_4$ (H_2O)	301 at 0.2	95% at 2 (1000)	[68]
TAQ-BQ	condensation reaction	cathode	2 M $ZnSO_4$ (H_2O)	208 at 0.1	87% at 1 (1000)	[88]
DAAQ-TFP-COF-GOPH	composite with GO	cathode	0.5 M $ZnSO_4$ + 0.5 M Li_2SO_4 (H_2O)	60 at 0.015	82% at 0.015 (500)	[77a]
COF	triazine based	cathode	0.5 M $Mg(TFSI)_2$ (DME)	107 at 0.02	99.4% at 0.57 (3000)	[70]
HATN-HHTP@CNT	growth on CNT	cathode	0.5 M $Mg(TFSI)_2$ (DME)	100 at 0.1	83.5% at 0.02 (150)	[76]
NPC COF-JLU2	carbonization	cathode	4 M KFSI (DME)	90 at 2	99% at 5 (30 000)	[72]
NPC COF-JLU2	carbonization	anode	1.3 M $AlCl_3$ ([EMIm]Cl)	250 at 0.1	94% at 1 (2500)	[72]
TpBpy-COF	condensation reaction	cathode	1.3 M $AlCl_3$ ([EMIm]Cl)	152 at 2	125% at 2 (13 000)	[73]
HATN-HHTP@CNT	growth on CNT	cathode	1.3 M $AlCl_3$ ([EMIm]Cl)	110 at 0.2	83% at 0.1 (350)	[76]

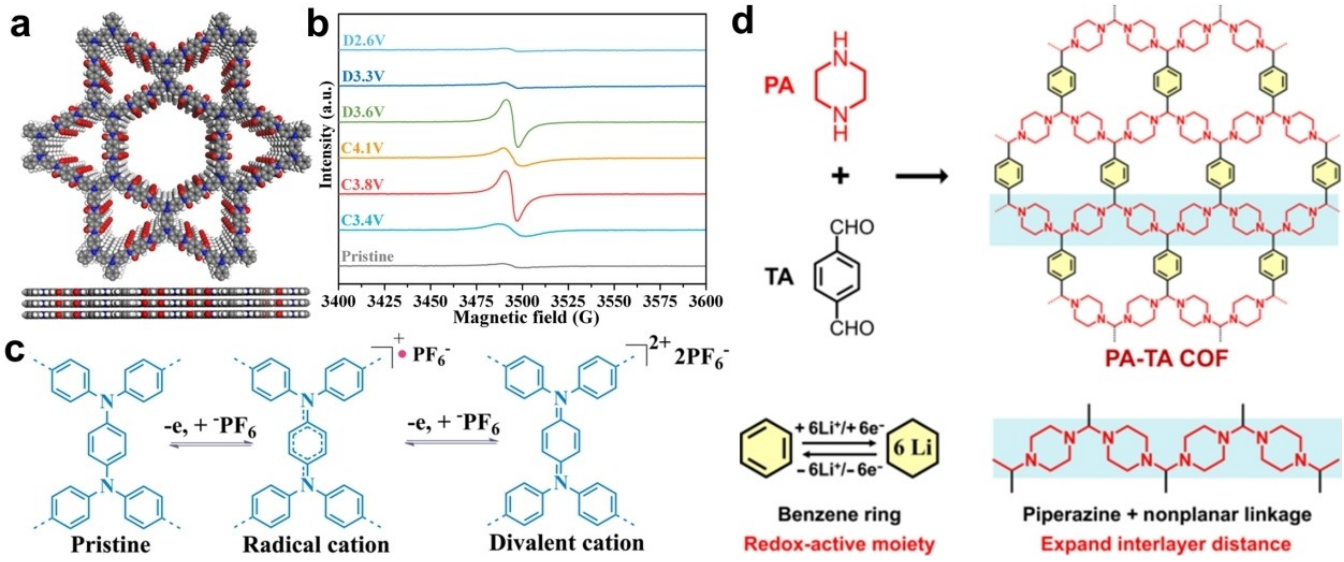

Figure 5. a) Chemical structures of TPPDA-PICOF. b) Ex-situ EPR spectra. c) Representative redox mechanism. Reproduced with permission from Ref. [48]. Copyright (2022) Royal Society of Chemistry. d) Schematic of the synthesis and the redox mechanism of PA-TA COF. Reproduced with permission from Ref. [49]. Copyright (2021) SpringerLink.

3.2. COFs for sodium-ion battery

Rechargeable sodium-ion batteries (SIBs) are expected to play a major role in the next generation metal-ion batteries because sodium is cheap and widely accessible. Compare with lithium ions, sodium and potassium ions possess larger ion sizes, and the larger ionic diameter limits the application of traditional electrode materials such as metal oxides and graphite. However, dissolution in organic electrolytes, low electronic conductivity, little redox stability, and many defects in the π-conjugated frameworks are the inherent problems of organic compounds. The adjustable pore size and topology structure make COFs electrode materials suitable for use in sodium ion batteries. Moreover, COFs with N-atom as redox site exhibit excellent electronic conductivity, which makes it possible to prepare sodium ion electrode materials with high capacity and rate performance.

Hani M. El-Kaderi et al. successfully synthesized the Aza-COF (Figure 8a) by 1,2,4,5-benzenetetramine tetrahydrochloride (TAB) and hexaketocyclohexane octahydrate (HKH).[55] As the cathode electrode material of sodium batteries, the Aza-COF with phenazine-decorated channels showed distinguished theoretical specific capacity of 603 mAh g^{-1} based on the 6-Na^+ reaction process (Figure 8b). Aze-COF exhibited prominent cycling stability, and the rechargeable capacity retained above 87% at current density 3 A g^{-1} for 500 cycles (Figure 8c).

Ramasamy Karvembu et al. reported a synthetic method centered on hexachlorophosphazene and linked by tris(2,3,6,7,10,11-hexahydroxytriphenylene of COIHP-1.[56] The splendid electrical conductivity of COIHP-1 achieved 9.52×10^{-3} S cm^{-1}. The storage mechanism of Na^+ in COIHP-1 was presumed to a 9 electrons and Na^+ ions progress (Figure 8d) connected with P=N units during the charging/discharging process. Thus, the theoretical specific capacity obtained by calculation was 333.6 mAh g^{-1}.

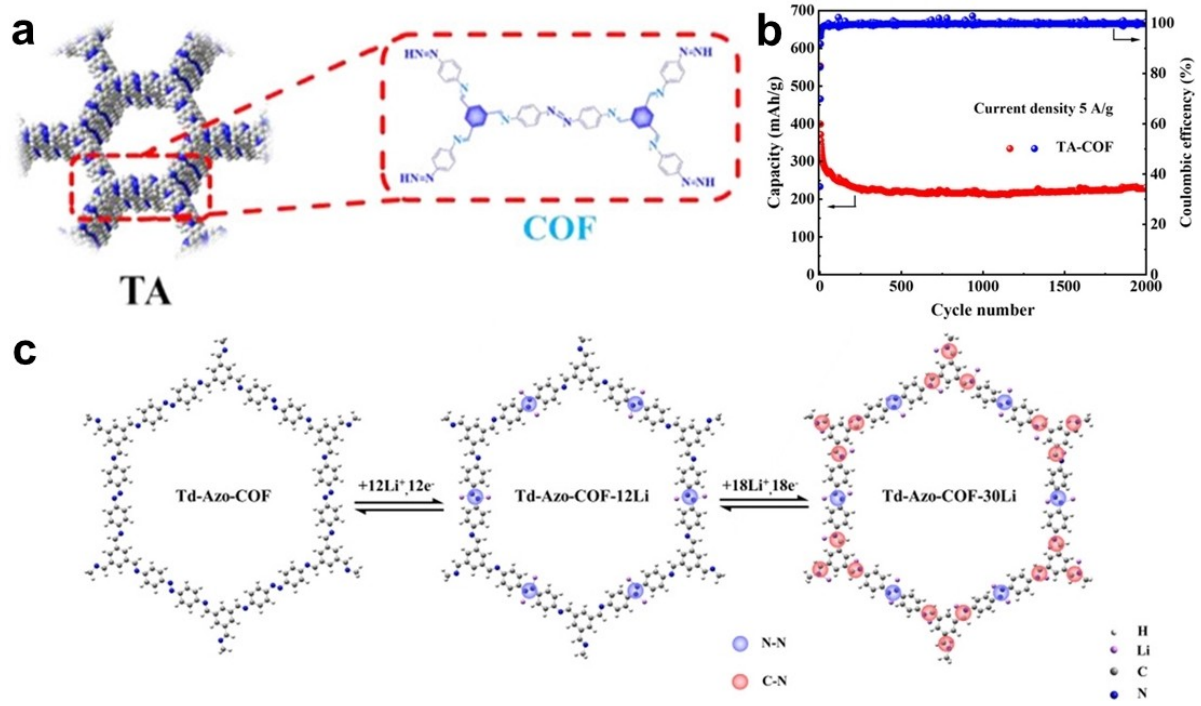

Figure 6. a) Chemical structures of TA COF. b) Cycling performance (5 A g^{-1}, 2000 cycles) and c) structural evolution of TA COF. Reproduced with permission from Ref. [50]. Copyright (2022) WILEY-VCH.

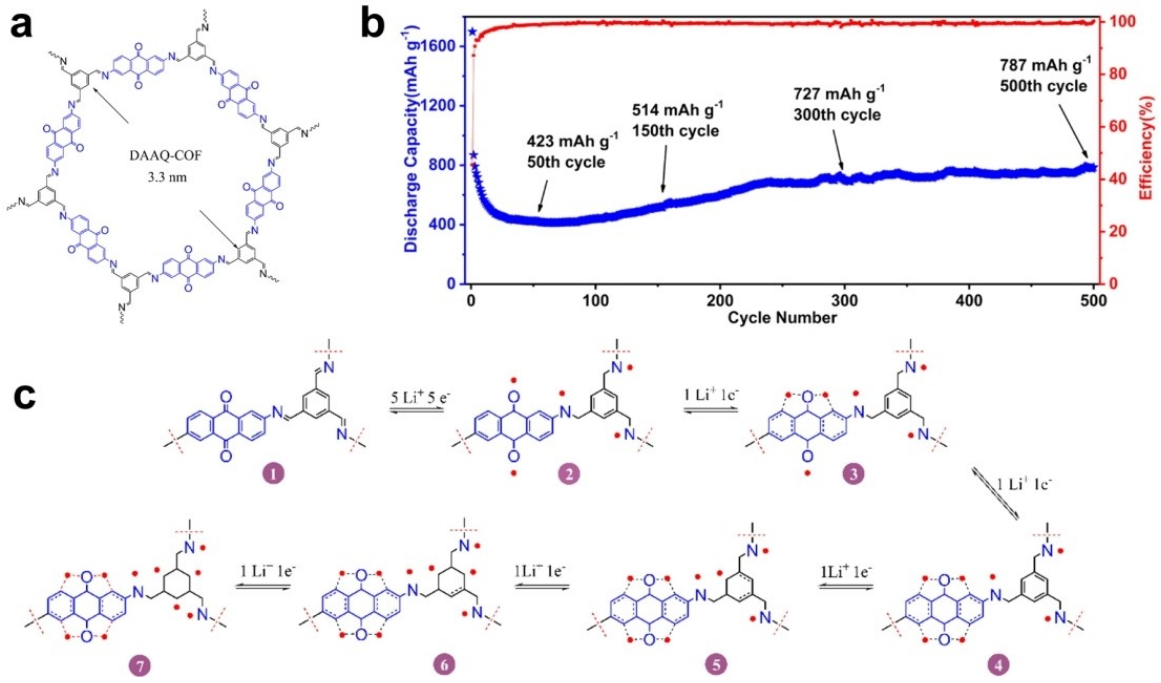

Figure 7. a) Chemical structures of DAAQ-COF. b) Cycling performance (1 A g^{-1}), and c) structural evolution mechanism of DAAQ-COF. Reproduced with permission from Ref. [52]. Copyright (2021) ACS Publications.

3.3. COFs for potassium-ion battery

Compared with other metal-ion batteries, the potassium-ion batteries (PIBs) possess relatively low redox potential of K/K^+ (−2.936 V vs. SHE), demonstrating the high voltage plateau and high energy density of PIBs. Moreover, K resource are cost-effective and abundant, leading PIBs as a promising alternative for LIBs.

Furthermore, the smallest Stokes radius (3.6 Å) of potassium ions compared to that of lithium ion (4.8 Å) and sodium ion

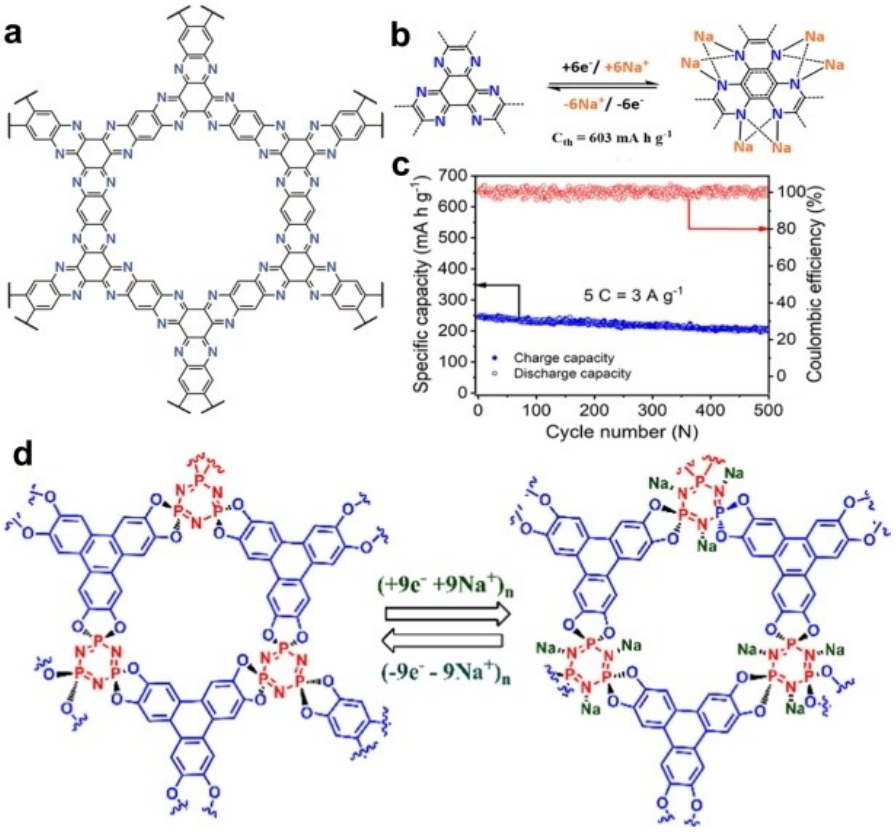

Figure 8. a) Chemical structure of Aza-COF. b) Structural evolution mechanism. and c) cycling performance (3 A g^{-1}) of Aza-COF. Reproduced with permission from Ref. [55]. Copyright (2021) American Chemical Society. d) Proposed Na^+ storage mechanism of COIHP-1. Reproduced with permission from Ref. [56]. Copyright (2022) American Chemical Society.

(4.6 Å) makes potassium ions have higher transfer number, ionic conductivity and mobility in the electrolyte, which exhibits distinguished dynamic performance for PIBs. Potassium ions can be easily insertion/extraction from the COFs structures to give a COF intercalation compound, thus showing good specific capacity and rate performance. However, the disadvantages of organic materials are obvious, and the problems of rapid decline in capacity and poor cycling stability performance need to be addressed urgently.

Psaras L. McGrier et al. reported two kinds of alkynyl-linked COFs (TAEB-COF and DBA-COF 3), which were constructed by dehydrobenzoannulene (DBA) and 1,3,5-tris(arylethynyl)benzene (TAEB) building blocks.[57] When applied as high concentration electrolyte for potassium-ion batteries (KIBs), TAEB-COF exhibited higher capacity and superior efficiency than DBA-COF 3. The activity of alkynyl groups in TAEB-COF (Figure 9a) contributed the process of K-ions insertion/extraction, which were confirmed by DFT calculations. TAEB-COF provided a high reversible capacity value of (254.0 mAh g^{-1} at 50 mAh g^{-1}) and excellent efficiency (100%) after 300 cycles (Figure 9b).

In order to solve the puzzle of solubility and dispersion of active groups, obtain remarkable stability and potassium diffusion coefficient, COFs were usually in-situ grown on CNT or graphite.[58] Xing-Long Wu group developed a P-COF@SWCNT (Figure 9c) based on single-walled carbon nanotubes (SWCNT) via amine and anhydride in-situ condensation reaction.[59] While comparing with P-COF, the P-COF@SWCNT demonstrated excellent stability and capacity (438 mAh g^{-1} at 50 mAh g^{-1}).

3.4. COFs for zinc-ion battery

As a new and promising alternative energy storage technology, zinc-ion rechargeable batteries have attracted much attention due to their abundant natural resources, cost effectiveness and inherent safety.[60] In particular, the application of aqueous electrolytes in zinc-ion batteries (ZIBs) solve the trickiest problem that organic molecules dissolved in traditional electrolyte.[61] The intercalation mechanism of Zn^{2+} ions during charging and discharging process has been discussed and revealed through density functional theory calculation and experimental analysis.[62] And beyond that, zinc ion rechargeable batteries shows great potential for portable electronic applications and large-scale energy storage systems.

In 2019, Banerjee et al. first reported a hydroquinone linked β-ketoenamine HqTp-COF (Hq-2,5-diaminohydroquinone, Tp-1,3,5-triformylphloroglucinol) as cathode material in an aqueous ZIBs. The zinc ion interaction mechanism in the adjacent layers of HqTp-COF was presented in Figure 10(a).[63] Since then, COF electrode materials have been widely researched for ZIBs. For example, a novel phenanthroline PA-COF demon-

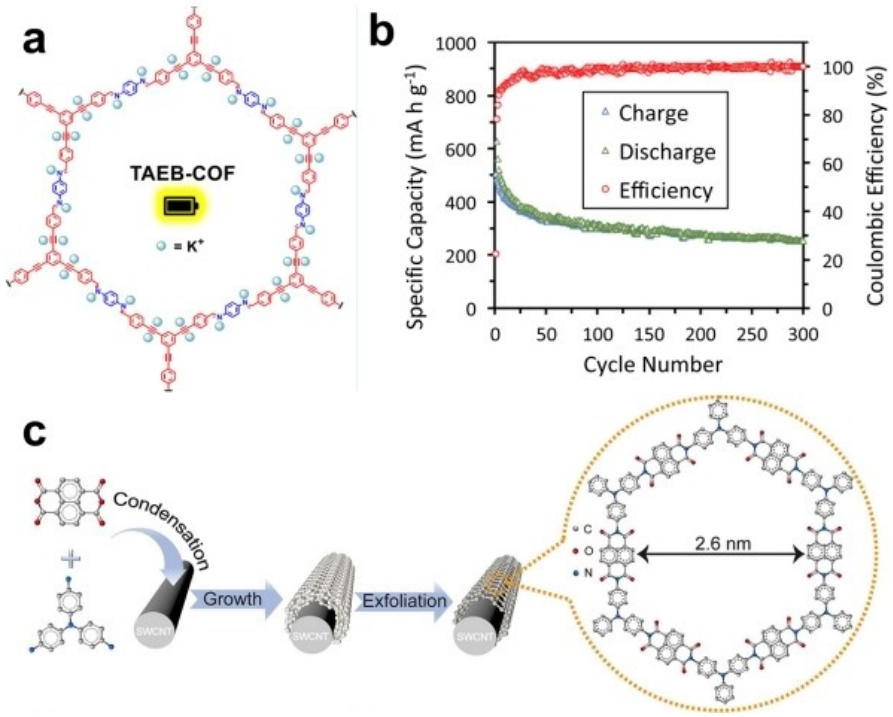

Figure 9. a) Chemical structure and of Aza-COF. b) Cycling performances for TAEB-COF at 50 mA g^{-1}. Reproduced with permission from Ref. [57]. Copyright (2021) American Chemical Society. c) synthetic method of P-COF@SWCNT. Reproduced with permission from Ref. [59]. Copyright (2022) Wiley-VCH.

strated the cointercalation of Zn^{2+} and H^+ during charging and discharging process in ZIBs (Figure 10b).[64] Subsequently, Alshareef et al. prepared 1,4,5,8,9,12-hexaazatriphenylene-based HAQ-COF with quinone group. The quinone groups introduced in the HAQ-COF significantly enhanced the average potential and storage capability for ZIBs (Figure 10c).[65] The carbonyl-based PI-COF was synthesized by using polyarylimide molecules (Feng et al.), and the two-step Zn^{2+} storage process in PI-COF was confirmed.[66] Tao et al. designed an orthoquinone-based BT-PTO COF with ultrahigh ZIBs performance.[67] In addition, they were the first to propose the co-insertion mechanism of BT-PTO COF that Zn^{2+} first followed by two H^+ during charging and discharging process. Besides, Liu et al. successfully synthesized a multiple carbonyl active sites Tp-PTO-COF with high specific capacities (301.4 mAh g^{-1} at 0.2 C).[68] The interaction mechanism of zinc ion in the adjacent layers and within layers for bilayer Tp-PTO-COF model fragment compound has been proposed (Figure 10d). The Zn_7@Tp-PTO model was identified as the most probable construction after full discharging.

In addition to the research focused on zinc ion electrolyte of aqueous electrolytes system, there are also some studies on electrolyte of organic electrolytes system, such as the influence of different solvation structures (polyethylene glycol (PEG) + H_2O, ethyl methyl carbonate (EMC) and acetonitrile(ACN)) on the voltage of organic electrodes.[69]

3.5. COFs for magnesium-ion battery

Magnesium-ion (Mg-ion) batteries have been regarded as one of the alternative energy storage technologies of Li-ion batteries and have attracted extensive attentions, because Mg is abundant, cost effective, highly safe (dendrite-free), and nearly twice volumetric capacity of Li anode. However, the Mg ion intercalation process suffered kinetic hysteresis, which leads to unsatisfactory electrochemical performance. In addition, organic electrode materials with more flexible Mg-ion migration paths and lower intermolecular forces are expected to improve the reaction kinetics and cyclic stability of Mg-ion batteries. However, in order to overcome the challenges of high solubility and low electronic conductivity of conventional organic electrolytes, COFs electrode materials have been developed continuously.

Chunsheng Wang et al. reported a porous COF (Figure 11a) based on benzene rings and triazine rings for Mg^{2+} storage cathodes.[70] The rate performance (0.2 to 20 C of current densities) was exhibited in Figure 11(b), the specific capacity retained 70% (current density from 0.2 C to 2 C) and 52% (current density from 0.2 C to 10 C), respectively. The specific capacity at 0.2 C was 107 mAh g^{-1}. Figure 10(c) shows the Mg-ion storage reaction and electrochemistry behaviors during the reversible process. The triazine-based COFs electrode exhibited excellent long-cycle stability and ultra-low capacity decay rate of Mg-ion battery. The average decay rate of each cycle was 0.0196% for 3000 cycles at the high rate of 5 C. The diople-quadrupole interaction of the lone pair electron of the nitrogen atom in the triazine ring increased the electronic conductivity

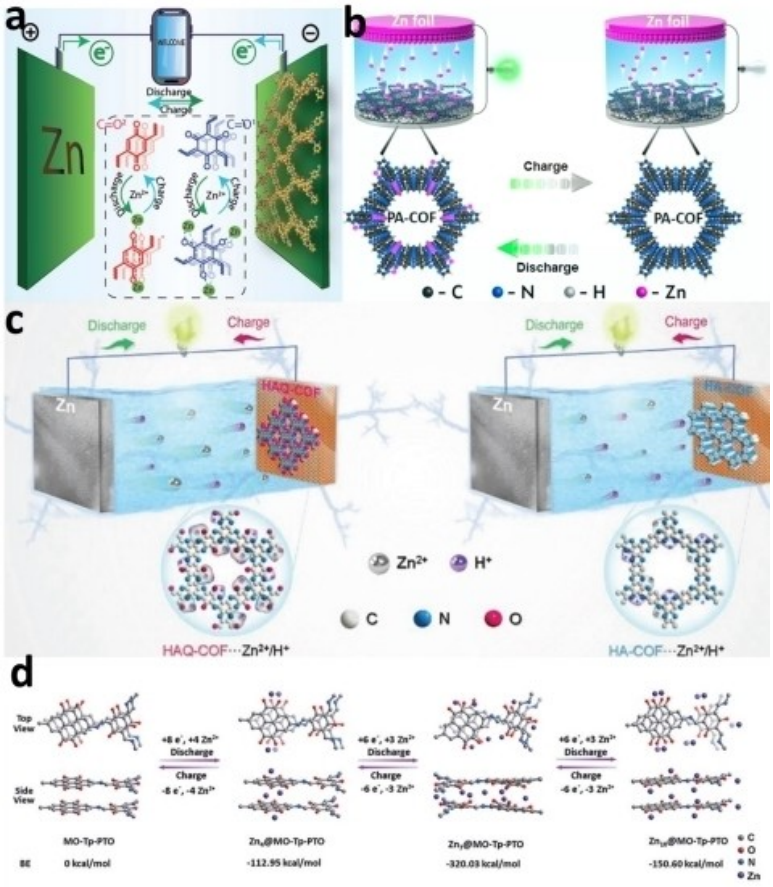

Figure 10. Application of COF cathodes materials in zinc-ion batteries. a) Schematic representation of HqTp-COF and zinc ion interaction mechanism in the adjacent layers of HqTp-COF. Reproduced with permission from Ref. [63]. Copyright (2019) The Royal Society of Chemistry. b) Schematic illustration of PA-COF electrochemical behavior in zinc ion supercapattery. Reproduced with permission from Ref. [64]. Copyright (2020) American Chemical Society. c) Schematic illustrations of functionalized group manipulate to increase Zn^{2+} storage in ZIBs for HAQ-COF and HA-COF. Reproduced with permission from Ref. [65]. Copyright (2021) Wiley-VCH. d) The binding energies calculation with different Zn^{2+} ions numbers of Tp-PTO-COF. Reproduced with permission from Ref. [66]. Copyright (2022) The Royal Society of Chemistry.

of the COF material. As the redox centers, the triazine rings activity units outstanding reaction kinetics and stability. Behnam Chameh et al. also confirmed electrochemical activity of triazine-based COF through DFT calculation.[71]

3.6. COFs for aluminum-ion battery

The electrode materials of aluminum-ion batteries have always been a research focus, but the traditional inorganic transition metal materials have limited theoretical capacity, serious volume expansion, slow redox kinetics and irreversible conversion reactions, which greatly limit the development of aluminum batteries. In contrast, organic electrode materials are economical and environmentally friendly, with abundant redox active sites, excellent electrochemical reversibility, and diversified structural design methods. Among them, quinone-based polymers containing carbonyl groups (C═O), as the most typical organic electrode materials, can store aluminum through complexation. However, the diffusion hysteresis of the huge aluminum ionic groups in the electrolyte can reduce the complexation efficiency with quinone-based electrodes. Although nitrogen-containing organic electrodes (C═N) have also been used in aluminum-ion batteries, they show low voltage plateau and unstable electrochemical performance.

Dongshan Zhou et al. firstly used the nitrogen-rich COF-JLU2 as the carbide source to prepare a nitrogen-doped porous carbon (NPC) aluminum electrode materials (Figure 12a).[72] Combined with the DFT calculation results, the NPC exhibited favorable conductivity and preponderant electron density distribution. The uniform distributed imine units on the NPC COF-JLU2 could promote the metal-ions/-electrons transport as well as the enhance the electrode conductivity. Based on the unique structural advantages of COF materials and the reversible active sites between C═O and C═N synergistic mechanism, the battery exhibited good reversibility. Ultrahigh coulombic efficiency has been demonstrated by the DFT cathode materials in Al-ion battery after 30 000 cycles (> 99 %).

The TpBpy-COF (Figure 12b) cathode materials, obtained by condensation reaction for 5,5′-diamino-2,2′-bipyridine (Bpy) and triformylphloroglucinol (Tp), was used for aluminum-ion batteries.[73] The stable structure of TpBpy-COF and stratifies

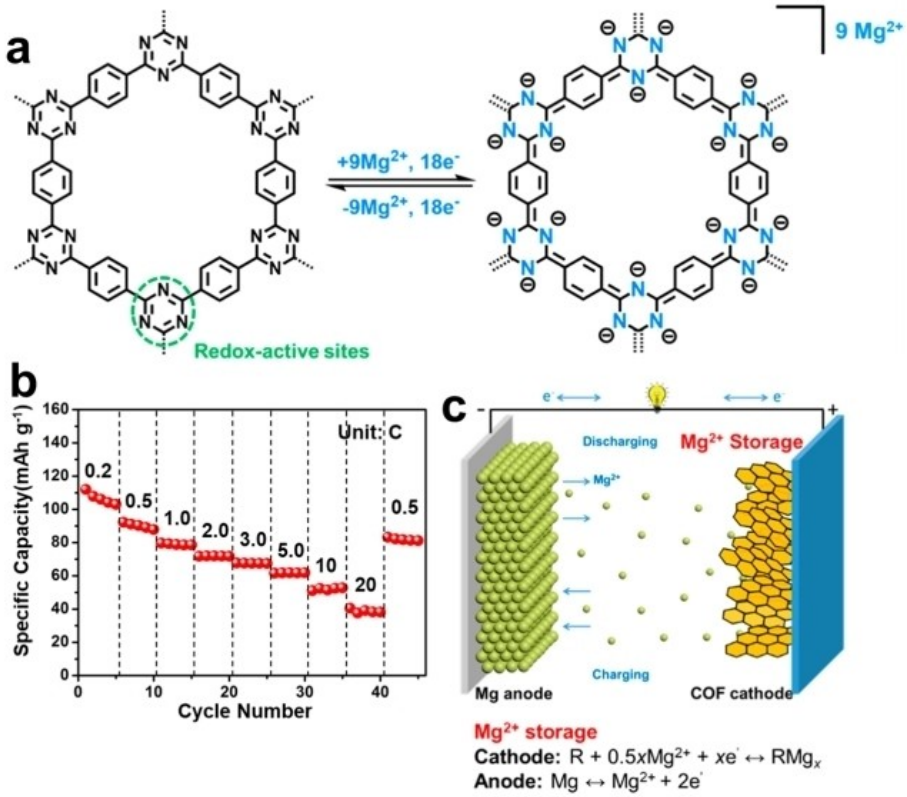

Figure 11. a) Chemical structure and possible electrochemical redox mechanism of the COF. b) Rate performance and c) schematic illustrations of the reaction mechanism of the COF. Reproduced with permission from Ref. [70]. Copyright (2020) American Chemical Society.

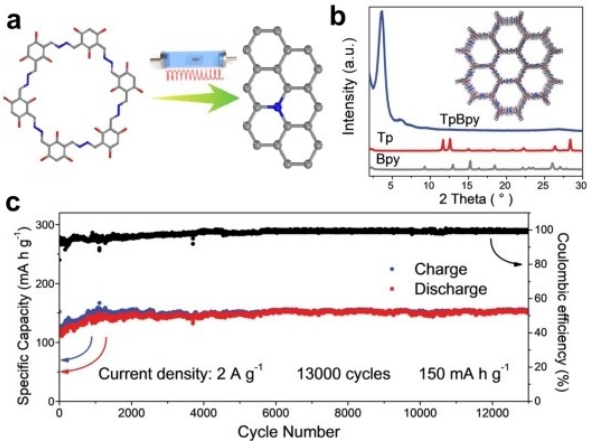

Figure 12. a) Chemical structure and Preparation procedure of NPC. Reproduced with permission from Ref. [72]. Copyright (2019) American Chemical Society. b) Structure and PXRD patterns of TpBpy-COF; c) cycling performances for TAEB-COF at 2000 mA g^{-1}. Reproduced with permission from Ref. [73]. Copyright (2020) Wiley-VCH.

pores with large surface area (1794 $m^2 g^{-1}$) allowed the rapid intercalation and diffusion of anions, making the synthesized COF possessed excellent long-term stability (Figure 12c) and Coulombic efficiency (150 mAh g^{-1} at 2 A g^{-1}, 13 000 cycles). The C=N groups in COFs not only formed a stable π-π conjugate system, but also assisted the adjacent C=O to combine the large volume $AlCl_4^-$ anion group, giving the COFs strong redox activity and excellent stability.

3.7. Characterization

The research and development of high-performance COF-based batteries, especially the systematic analysis about composition, morphology, chemical structure and electrochemical performance of COF electrode materials during the charging and discharging process, requires suitable modern characterization analysis technology. On the one hand, it is necessary to obtain the basic electrochemical data of the COF battery, such as capacity, energy density, voltage platform, cycle stability, etc. On the other hand, a series of characterization methods are applied to research the electrochemistry mechanism, so as to guide the optimization and improvement of COF battery design and obtain COF electrode materials with better performance. The COF electrode materials characterization techniques mainly include electrochemical performance testing, microanalysis, X-ray diffraction (XRD) characterization analysis, electron paramagnetic resonance (EPR), nuclear magnetic resonance (NMR) and fourier transform infrared spectroscopy (FT-IR) technology, etc., which are used to test the COF electrode materials from different scales.

Further improvement of COF organic batteries requires an in-depth understanding of the underlying redox reactions and

active-material degradation mechanisms. Advanced characterization techniques, especially in situ/in operando characterization tools, are used and developed in the field of COF organic batteries to probe the rate-limiting performance and design characteristics of functional materials.

To further improve the electrochemical performance of COF-based ionic batteries, in-depth understanding of the electrochemical reaction and electrode failure mechanism is critically required. Application of advanced in-situ/operando characterization techniques to probe electrode materials during charge/rechargeable process are developed in COF-based ionic batteries and have made significant progress of COF-based electrode materials. Yong Wang et al. successfully verified the of translation active sites (C═O) in DAAQ-TFP-COF through in-situ FT-IR spectra (Figure 13a).[74] The disappeared/reappeared processes of characteristic peak ($\approx$1610 cm^{-1}) confirm that the C═O active site is a reversible store point for Li ions. Furthermore, the in-situ FT-IR confirms the transformation of C═N functional group (around 1620 cm^{-1}) in triazine-based covalent organic framework (DCB-COF) electrodes.[75] The in-situ FT-IR test results proved that C═N group gradually transform into –C–N–Li ionic bonds during the lithium insertion process.

Jun Yang et al. detect azo active groups translation in Azo-CTF during reversable process through in-situ Raman technology (Figure 13b).[76] According to the results of in-situ Raman spectroscopy, the absorption peak of N═N (1450 cm^{-1}) became weaker while the peak of Li-N–N-Li (1408 cm^{-1}) enhanced from 2.9 V to 1.2 V during discharge process. In the near future, in-situ technology will be widely used to research the mechanism of COF metal-ion batteries. In addition, in-situ Raman characterizations proved that the formation and evolution of C–C (benzyl) to α-C radical intermediate on the CTF-p during charge/discharge cycling.[22]

4. Conclusion and Perspective

Covalent organic frameworks (COFs) are crystalline porous organic materials with 2D or 3D frame structure, which have broad application prospects. Based on the ample design synthesis strategies, the construction elements with different angle distribution, symmetry, linker length and geometric shape can be selected to form COFs with abundant topological structure. Meanwhile, the structure design and introduction of functional groups to regulate the electrochemical properties provides more possibilities for COF electrode materials, laying a solid foundation for their practical application. This paper reviews the basic topological structure design of COFs and their application in multi-valent metal-ion storage. Table 1 summarizes the design strategies, cyclic performances and electrolyte compositions of COFs electrode materials used in metal-ion (Li^+, Na^+, K^+, Zn^{2+}, Mg^{2+} and Al^{3+}) batteries in the recent years.

COFs possess the definite crystal structures, which can reveal the conduction mechanism of metal-ions in the channel at the molecular level. Although COFs electrode materials have shown great potential in metal-ion batteries due to their inherent advantages, the organic research on high performance metal-ion batteries is still in its infancy. In order to make COFs better served metal-ion batteries, some typical common methods to improve electrochemical performance were summarized as follows:

1. The stability of COFs intermediates can be improved by increasing the size of conjugate element. In order to further improve the comprehensive performance of COFs batteries, it is necessary to have a deep understanding of the redox process upon charging and discharging. However, due to the instability of organic radical intermediates, it is a big challenge to directly observe the structural evolution during charging and discharging process by the general characterization techniques. Increasing the size of the conjugated units can effectively delocalize the radical electrons to

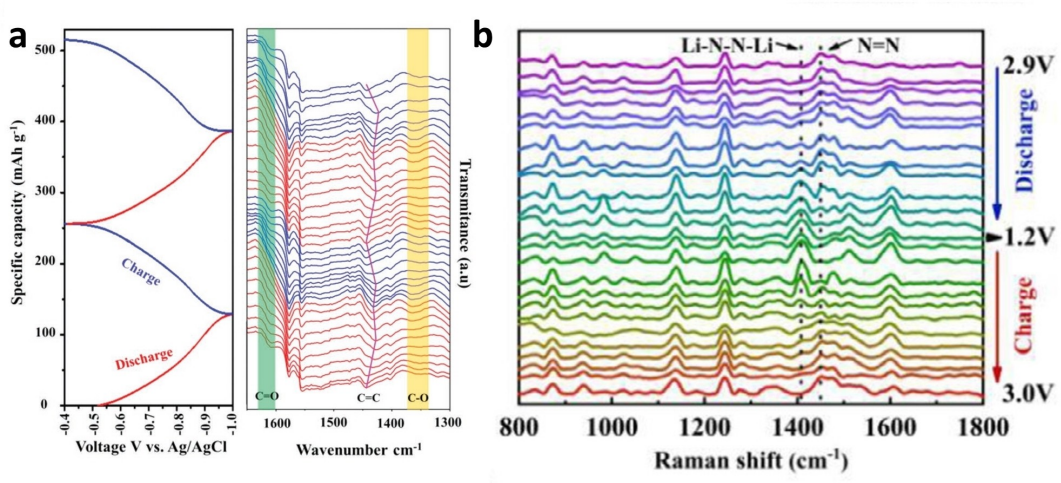

Figure 13. a) GCD curves of DAAQ-TFP-COF electrode at 0.5 A g^{-1} in the initial two cycles and the corresponding in situ FT-IR spectra collected at different potentials. Reproduced with permission from Ref. [74]. Copyright (2022) Wiley-VCH. b) In situ Raman spectroscopy of Azo-CTF electrodes. Reproduced with permission from Ref. [86]. Copyright (2021) Elsevier.

reduce the side reaction of the intermediates and thus enhance the cycling stability of the COFs electrodes. The COFs can be prepared by selecting precursors with large size π-π conjugate building blocks. In addition, the ordered π-π conjugated structure in the COFs provides a way for efficient electron transport, and the regular pore arrangement provides a way for enhanced ion diffusion.

2. Increasing the number and utilization of redox active sites can increase the capacity of COFs. The regulatory mechanism and preparation methods of COFs materials are still imperfect, resulting in defects in the cycling stability and energy density of COF electrode materials in the charging and discharging process of metal-ion batteries. By appropriately increasing the size of the channel diameter of COFs, the ion migration efficiency can be improved and more active sites can be exposed, so as to raise the theoretical capacity and long-term cycle stability of the battery.[89] In addition, the development and preparation of COFs electrode materials with various active sites can greatly increase the theoretical capacity of COF batteries.
3. The poor electronic conductivity of organic materials will affect the electron transport inside the electrodes and thus reduce the rate performance and reversible capacity of the batteries. The conductivity can be enhanced by introducing conductive element skeletons, such as thiophene, pyrrole and other groups. In addition, CNT, graphene or other carbon materials are introduced as the carrier to compound with COFs to enhance the conductivity, and increase the capacity and high-rate stability.[77,53] By eliminating the influence of activation process of COFs material during charging and discharging, the electrode sheet can be infiltrated in the electrolyte for a period of time in advance. By fully contacting the electrode with the electrolyte, the huge fluctuation of the battery in the initial stage of testing is eliminated.
4. To accelerate the building blocks selection and reduce the trial and error cost through theoretical calculation. Theoretical simulations or machine learning can be used to predict and confirm the active sites of COFs and to understand the radical transition during charging/discharging mechanisms. By establishing the relationship between structure and performance through traditional algorithm and model construction, targeted design and rapid screening of organic electrode materials can be realized.

From the development of COF materials, it can be seen that in recent years, diversified novel COFs have been successfully prepared. The electrochemistry characterization and testing of COF in metal-ion batteries have gradually enriched the database. With the increasing variety of COFs and extensive applications in the metal-ion battery field, COFs electrode materials show immeasurable application potentials. However, the breakthrough of COFs batteries performance and the wide applications on metal-ion batteries are still in the infancy and facing lots of challenges. Firstly, it is necessary to ensure the crystallinity of COFs in synthesis process. Through reasonable molecular design strategy, appropriate redox active groups are introduced into COFs, so that COF electrode materials can be used as electrode active materials with excellent electrochemical properties, which is still to be developed. At present, topological materials with other connected 2D-COF or 3D structure are rarely studied, and the types of COFs need to be expanded. Secondly, the development of COFs with distinguished conductivity is essential to improve the Coulombic efficiency and energy density of metal-ion batteries. Most of the COF-based electrodes reported so far exhibit poor conductivity, which limits the specific capacity greatly. In addition, how to process COFs to expose more active sites is also worth further consideration. Finally, the mechanism of COFs in various metal-ion batteries should be better understood. It should be combined with modern characterization techniques to further understand the dynamic mechanism of COF and analyze the transformation of COF during the energy storage process of metal-ion batteries.

The design, synthesis, functionalization and development of various electrochemical properties require the unremitting efforts of many researchers. COFs electrode materials have great development space in metal-ion batteries, and have broad application prospects in large-scale energy storage applications in the near future.

Acknowledgements

The authors thank the supports from the National Natural Science Foundation of China (No. 21875097), Basic Research Project of the Science and Technology Innovation Commission of Shenzhen (No. JCYJ20200109141640095), and Shenzhen Key Laboratory of Interfacial Science and Engineering of Materials (No. ZDSYS20200421111401738).

Conflict of Interest

The authors declare no conflict of interest.

Keywords: covalent organic framework (COFs) · electrochemical performance · metal-ion batteries · regulate and control · topological structure

[1] a) S. Gu, Y. T. Chen, R. Hao, J. Zhou, I. Hussain, N. Qing, M. Li, J. J. Chen, Z. Wang, W. Zheng, Q. M, Gan, Z. Q. Li, H. Guo, Y. Z. Li, K. L. Zhang, Z. G. Lu, *Chem. Commun.* **2021**, *57*, 7810–7813; b) T. Shao, Y. Zhang, T. Cao, Y. T. Yang, Z. Li, H. M. Liu, Y. G. Wang, Y. Y. Xia, *Chem. Eng. J.* **2022**, *431*, 133735; c) C. L. Wei, L. W. Tan, Y. C. Zhang, B. J. Xi, S. L. Xiong, J. K. Feng, *ACS Appl. Mater. Interfaces* **2022**, *14*, 2979–2988.
[2] a) L. Croguennec, M. R. Palacin, *J. Am. Chem. Soc.* **2015**, *137*, 3140–3156; b) F. Wan, Y. Zhang, L. L. Zhang, D. B. Liu, C. D. Wang, L. Song, Z. Q. Niu, J. Chen, *Angew. Chem. Int. Ed.* **2019**, *58*, 7062–7067; *Angew. Chem.* **2019**, *131*, 7136–7141; c) Y. Wang, T. Wang, J. Q. Lei, K. J. Chen, *Inorg. Chem. Front.* **2021**, *8*, 3325–3335; d) R. Hao, S. Gu, J. Chen, Z. Wang, Q. Gan, Z. Wang, Y. Huang, P. Liu, K. Zhang, K. Liu, C. Liu, Z. Lu, *Mater. Today Energy* **2021**, *21*, 100826.
[3] a) T. P. Nguyen, A. D. Easley, N. Kang, S. Khan, S. Lim, Y. H. Rezenom, S. Wang, D. K. Tran, J. Fan, R. A. Letteri, X. He, L. Su, C. H. Yu, J. L. Lutkenhaus, K. L. Wooley, *Nature* **2021**, *593*, 61–66; b) Z. Li, J. Guo, Y. Wan, Y. Qin, M. Zhao, *Nano Res.* **2022**, *15*, 3514–3532; c) S. Chen, Y.

Feng, J. Wang, E. Zhang, X. Yu, B. Lu, *Sci. China Mater.* **2021**, *64*, 547–556.
[4] a) J. A. R. Navarro, *Science* **2018**, *361*, 6397; b) K. S. Song, S. N. Talapaneni, T. Ashirov, A. Coskun, *ACS Appl. Mater. Interfaces* **2021**, *13*, 26102–26108; c) X. Cui, H. Dong, S. Chen, M. Wu, Y. Wang, *Batteries & Supercaps* **2021**, *4*, 72–97.
[5] a) Q. Zhu, A. R. B. Méndez, L. Cheng, J. F. Diaz, E. M. Sandoval, F. L. Urias, J. Wang, J. F. Gohy, J. C. Charlier, A. Vlad, *Nano Sel.* **2022**, *3*, 864–873; b) A. L. Chen, N. Shang, Y. Ouyang, L. Mo, C. Zhou, W. W. Tjiu, F. Lai, Y. E. Miao, T. Liu, *eScience* **2022**, *2*, 192–200.
[6] a) A. P. Côté, A. I. Benin, N. W. Ockwig, M. O'Keeffe, A. J. Matzger, O. M. Yaghi, *Science* **2005**, *310*, 1166–1170; b) W. Wang, C. Zhao, J. Yang, P. Xiong, H. Su, Y. Xu, *Sci. China Mater.* **2021**, *64*, 2938–2948; c) S. Xu, H. Dai, S. Zhu, Y. Wu, M. Sun, Y. Chen, K. Fan, C. Zhang, C. Wang, W. Hu, *eScience* **2021**, *1*, 60–68.
[7] a) T. Sun, J. Xie, W. Guo, D. S. Li, Q. Zhang, *Adv. Energy Mater.* **2020**, *10*, 1904199; b) J. J. Chen, S. Gu, R. Hao, Z. Y. Wang, M. Q. Li, Z. Q. Li, K. Liu, K. M. Liao, Z. Q. Wang, H. Huang, Y. Z. Li, K. L. Zhang, Z. G. Lu, *Rare Met.* **2022**, *41*, 2055–2062.
[8] a) N. Liu, L. Shi, X. Han, Q. Y. Qi, Z. Q. Wu, X. Zhao, *Chin. Chem. Lett.* **2020**, *31*, 386–390; b) T. Sun, Q. Q. Sun, Y. Yu, X. B. Zhang, *eScience* **2021**, *1*, 186–193; c) J. Chen, S. Gu, R. Hao, K. Liu, Z. Wang, Z. Li, H. Yuan, H. Guo, K. Zhang, Z. Lu, *ACS Appl. Mater. Interfaces* **2022**, *14*, 44330–44337.
[9] a) G. Li, B. Zhang, J. Wang, H. Zhao, W. Ma, L. Xu, W. Zhang, K. Zhou, Y. Du, G. He, *Angew. Chem. Int. Ed.* **2019**, *58*, 8468–8473; *Angew. Chem.* **2019**, *131*, 8556–8561; b) T. Cai, Y. Han, Q. Lan, F. Wang, J. Chu, H. Zhan, Z. Song, *Energy Storage Mater.* **2020**, *31*, 318–327; c) C. Ding, C. Li, H. Tian, Y. Tong, W. Huang, Q. Zhang, *Batteries & Supercaps* **2022**, *5*, e202200160.
[10] S. Gu, S. Wu, L. Cao, M. Li, N. Qin, J. Zhu, Z. Wang, Y. Li, Z. Li, J. Chen, Z. Lu, *J. Am. Chem. Soc.* **2019**, *141*, 9623–9628.
[11] a) J. Wang, X. Liu, H. Jia, P. Apostol, X. Guo, F. Lucaccioni, X. Zhang, Q. Zhu, C. Morari, J. F. Gohy, A. Vlad, *ACS Energy Lett.* **2022**, *7*, 668–674; b) X. Yang, Y. Hu, N. Dunlap, X. Wang, S. Huang, Z. Su, S. Sharma, Y. Jin, F. Huang, X. Wang, S. Lee, W. Zhang, *Angew. Chem. Int. Ed.* **2020**, *59*, 20385–20389; *Angew. Chem.* **2020**, *132*, 20565–20569.
[12] a) Y. Liang, Y. Yao, *Joule* **2018**, *2*, 1690–1706; b) W. Yang, H. Yang, H. Zhou, *Batteries & Supercaps* **2022**, *5*, e202200197; c) X. Wang, H. Dong, A. E. Lakraychi, Y. Zhang, X. Yang, H. Zheng, X. Han, X. Shan, C. He, Y. Yao, *Mater. Today* **2022**, *55*, 29–36.
[13] C. Wei, L. Tan, Y. Zhang, K. Zhang, B. Xi, S. Xiong, J. Feng, Y. Qian, *ACS Nano* **2021**, *15*, 12741–12767.
[14] Z. Li, Z. W. Liu, Z. Li, T. X. Wang, F. Zhao, X. Ding, W. Feng, B. H. Han, *Adv. Funct. Mater.* **2020**, *30*, 1909267.
[15] X. Li, H. Wang, H. Chen, Q. Zheng, Q. Zhang, H. Mao, Y. Liu, S. Cai, B. Sun, C. Dun, M. P. Gordon, H. Zheng, J. A. Reimer, J. J. Urban, J. Ciston, T. Tan, E. M. Chan, J. Zhang, Y. Liu, *Chem* **2020**, *6*, 933–944.
[16] M. Tang, N. N. Bui, J. Zheng, L. Song, Y. Y. Hu, *J. Energy Chem.* **2021**, *60*, 9–15.
[17] Y. Ni, F. G. Gamez, M. P. Alvarez, Z. Nan, Z. Li, S. Wu, Y. Han, J. Casado, J. Wu, *J. Am. Chem. Soc.* **2020**, *142*, 12730–12742.
[18] W. Sun, J. Zhang, M. Xie, D. Lu, Z. Zhao, Y. Li, Z. Cheng, S. Zhang, H. Chen, *Nano Lett.* **2020**, *20*, 8120–8126.
[19] a) C. Z. Guan, D. Wang, L. J. Wan, *Chem. Commun.* **2012**, *48*, 2943–2945; b) J. Wang, N. Li, Y. Xu, H. Pang, *Chem. Eur. J.* **2020**, *26*, 6402–6422; c) C. J. Yao, Z. Wu, J. Xie, F. Yu, W. Guo, Z. J. Xu, D. S. Li, S. Zhang, Q. Zhang, *ChemSusChem* **2020**, *13*, 2457–2463.
[20] a) P. She, Y. Qin, X. Wang, Q. Zhang, *Adv. Mater.* **2022**, *34*, 2101175; b) S. Kandambeth, K. Dey, R. Banerjee, *J. Am. Chem. Soc.* **2019**, *141*, 1807–1822.
[21] a) P. Kuhn, M. Antonietti, A. Thomas, *Angew. Chem. Int. Ed.* **2008**, *47*, 3450–3453; *Angew. Chem.* **2008**, *120*, 3499–3502; b) E. Jin, M. Asada, Q. Xu, S. Dalapati, M. A. Addicoat, M. A. Brady, H. Xu, T. Nakamura, T. Heine, Q. Chen, D. L. Jiang, *Science* **2017**, *357*, 673–676; c) F. Jiang, Y. Wang, T. Qiu, Y. Zhang, W. Zhu, C. Yang, J. Huang, Z. Fang, G. Dai, *ACS Appl. Mater. Interfaces* **2021**, *13*, 48818–48827.
[22] Z. Q. Wang, S. Gu, L. J. Cao, L. Kong, Z. Y. Wang, N. Qin, M. Q. Li, W. Luo, J. J. Chen, S. S. Wu, G. Y. Liu, H. M. Yuan, Y. F. Bai, K. Zhang, Z. G. Lu, *ACS Appl. Mater. Interfaces* **2021**, *13*, 514–521.
[23] J. H. Park, C. H. Lee, J. M. Ju, J. H. Lee, J. Seol, S. U. Lee, J. H. Kim, *Adv. Funct. Mater.* **2021**, *31*, 2101727.
[24] a) X. Guan, H. Li, Y. Ma, M. Xue, Q. Fang, Y. Yan, V. Valtchev, S. Qiu, *Nat. Chem.* **2019**, *11*, 587–594; b) S. Xu, G. Wang, B. P. Biswal, M. Addicoat, S. Paasch, W. Sheng, X. Zhuang, E. Brunner, T. Heine, R. Berger, X. Feng, *Angew. Chem. Int. Ed.* **2019**, *131*, 859–863.
[25] a) F. Yu, W. Liu, B. Li, D. Tian, J. L. Zuo, Q. Zhang, *Angew. Chem. Int. Ed.* **2019**, *58*, 16101–16104; *Angew. Chem.* **2019**, *131*, 16247–16250; b) S. Haldar, D. Kaleeswaran, D. Rase, K. Roy, S. Ogale, R. Vaidhyanathan, *Nanoscale Horiz.* **2020**, *5*, 1264–1273; c) L. Sheng, L. Wang, J. Wang, H. Xu, X. He, *Chem. Commun.* **2020**, *56*, 10465–10468.
[26] T. Kim, S. H. Joo, J. Gong, S. Choi, J. H. Min, Y. Kim, G. Lee, E. Lee, S. Park, S. K. Kwak, H. S. Lee, B. S. Kim, *Angew. Chem.* **2022**, *134*, e202113780.
[27] J. Fan, T. Wang, B. P. Thapaliya, L. Qiu, M. Li, Z. Wang, T. Kobayashi, I. Popovs, Z. Yang, S. Dai, *Angew. Chem. Int. Ed.* **2022**, e202207607.
[28] J. Feng, M. Li, *Adv. Funct. Mater.* **2020**, 2001502.
[29] a) H. Wei, S. Chai, N. Hu, Z. Yang, L. Wei, L. Wang, *Chem. Commun.* **2015**, *51*, 12178–12181; b) S. T. Yang, J. Kim, H. Y. Cho, S. Kim, W. S. Ahn, *RSC Adv.* **2012**, *2*, 10179–10181.
[30] X. Feng, X. Ding, D. Jiang, *Chem. Soc. Rev.* **2012**, *41*, 6010–6022.
[31] a) M. A. Khayum, S. Kandambeth, S. Mitra, S. B. Nair, A. Das, S. S. Nagane, R. Mukherjee, R. Banerjee, *Angew. Chem. Int. Ed.* **2016**, *55*, 1–6; *Angew. Chem.* **2016**, *128*, 1–1; b) C. Liang, H. Lin, Q. Wang, E. Shi, S. Zhou, F. Zhang, F. Qu, G. Zhu, *J. Hazard. Mater.* **2020**, *381*, 120983.
[32] a) C. Zhao, C. S. Diercks, C. Zhu, N. Hanikel, X. Pei, O. M. Yaghi, *J. Am. Chem. Soc.* **2018**, *140*, 16438–16441; b) S. B. Alahakoon, C. M. Thompson, A. X. Nguyen, G. Occhialini, G. T. McCandless, R. A. Smaldone, *Chem. Commun.* **2016**, *52*, 2843–2845.
[33] Z. Cheng, M. Xie, Y. Mao, J. Ou, S. Zhang, Z. Zhao, J. Li, F. Fu, J. Wu, Y. Shen, D. Lu, H. Chen, *Adv. Energy Mater.* **2020**, 1904230.
[34] a) E. R. Wolfson, N. Xiao, L. Schkeryantz, W. K. Haug, Y. Wu, P. L. M. Grier, *Mol. Syst. Des. Eng.* **2020**, *5*, 97–101; b) Y. Zeng, R. Zou, Z. Luo, H. Zhang, X. Yao, X. Ma, R. Zou, Y. Zhao, *J. Am. Chem. Soc.* **2015**, *137*, 1020–1023.
[35] a) J. Li, F. Q. Zhang, F. Li, Z. Wu, C. Ma, Q. Xu, P. Wang, X. M. Zhang, *Chem. Commun.* **2020**, *56*, 2747–2750; b) Q. Song, S. Jiang, T. Hasell, M. Liu, S. Sun, A. K. Cheetham, E. Sivaniah, A. I. Cooper, *Adv. Mater.* **2016**, *28*, 2629–2637; c) F. Yu, W. Liu, S. W. Ke, M. Kurmoo, J. L. Zuo, Q. Zhang, *Nat. Commun.* **2020**, *11*, 5534.
[36] V. A. Kuehl, P. H. H. Duong, D. Sadrieva, S. A. Amin, Y. She, K. D. L. Oakey, J. L. Yarger, B. A. Parkinson, J. O. Hoberg, *ACS Appl. Mater. Interfaces* **2021**, *13*, 37494–37499.
[37] R. R. Liang, S. Y. Jiang, R. H. A, X. Zhao, *Chem. Soc. Rev.* **2020**, *49*, 3920–3951.
[38] a) N. Huang, L. Zhai, D. E. Coupry, M. A. Addicoat, K. Okushita, K. Nishimura, T. Heine, D. Jiang, *Nat. Commun.* **2016**, *27*, 12325; b) Z. F. Pang, S. Q. Xu, T. Y. Zhou, R. R. Liang, T. G. Zhan, X. Zhao, *J. Am. Chem. Soc.* **2016**, *138*, 4710–4713.
[39] H. M. E. Kaderi, J. R. Hunt, J. L. M. Cortés, A. P. Côté, R. E. Taylor, M. O'Keeffe, O. M. Yaghi, *Science* **2007**, *316*, 268.
[40] T. Ma, E. A. Kapustin, S. X. Yin, L. Liang, Z. Zhou, J. Niu, L. H. Li, Y. Wang, J. Su, J. Li, X. Wang, W. D. Wang, W. Wang, J. Sun, O. M. Yaghi, *Science* **2018**, *361*, 48–52.
[41] a) Q. Zhu, X. Wang, R. Clowes, P. Cui, L. Chen, M. A. Little, A. I. Cooper, *J. Am. Chem. Soc.* **2020**, *142*, 16842–16848; b) X. Yang, Y. Hu, N. Dunlap, X. Wang, S. Huang, Z. Su, S. Sharma, Y. Jin, F. Huang, X. Wang, S. Lee, W. Zhang, *Angew. Chem. Int. Ed.* **2020**, *59*, 20385–20389; *Angew. Chem.* **2020**, *132*, 20565–20569.
[42] a) X. Yang, Y. Hu, N. Dunlap, X. Wang, S. Huang, Z. Su, S. Sharma, Y. Jin, F. Huang, X. Wang, S. H. Lee, W. Zhang, *Angew. Chem.* **2020**, *132*, 20565–20569; *Angew. Chem. Int. Ed.* **2020**, *59*, 20385–20389; b) Z. A. Ghazi, L. Zhu, H. Wang, A. Naeem, A. M. Khattak, B. Liang, N. A. Khan, Z. Wei, L. Li, Z. Tang, *Adv. Energy Mater.* **2016**, *6*, 1601250; c) S. Lee, G. Kwon, K. Ku, K. Yoon, S. K. Jung, H. D. Lim, K. Kang, *Adv. Mater.* **2018**, *30*, 1704682; d) H. Yang, S. Zhang, L. Han, Z. Zhang, Z. Xue, J. Gao, Y. Li, C. Huang, Y. Yi, H. Liu, Y. Li, *ACS Appl. Mater. Interfaces* **2016**, *8*, 5366–5375.
[43] a) Y. Ding, X. Ren, D. Chen, F. Wen, T. Li, F. Xu, *ACS Appl. Energ. Mater.* **2022**, *5*, 3004–3012; b) K. Sakaushi, G. Nickerl, F. M. Wisser, D. N. Hamane, E. Hosono, H. Zhou, S. Kaskel, J. Eckert, *Angew. Chem. Int. Ed.* **2012**, *51*, 7850–7854; *Angew. Chem.* **2012**, *124*, 7972–7976; c) Y. Deng, C. Teng, Y. Wu, K. Zhang, L. Yan, *ChemSusChem* **2022**, *15*, e202102710.
[44] a) H. Yang, P. Fan, S. Liu, J. Wei, S. Tan, Q. Wang, H. Hou, *Int. J. Electrochem. Sci.* **2018**, *13*, 2606–2616; b) J. Xie, Z. Wang, Z. J. Xu, Q. Zhang, *Adv. Energy Mater.* **2018**, *8*, 1703509; c) J. Hu, Y. Liu, N. Liu, J. Li, C. Ouyang, *Phys. Chem. Chem. Phys.* **2020**, *22*, 3281–3289.
[45] S. Gu, X. Ma, J. Chen, R. Hao, Z. Wang, N. Qin, W. Zheng, Q. Gan, W. Luo, M. Li, Z. Li, K. Liao, H. Guo, G. Liu, K. Zhang, Z. Lu, *J. Energy Chem.* **2022**, *69*, 428–433.

[46] V. Singh, J. Kim, B. Kang, J. Moon, S. Kim, W. Y. Kim, H. R. Byon, *Adv. Energy Mater.* **2021**, *11*, 2003735.
[47] S. Jhulki, C. H. Feriante, R. Mysyk, A. M. Evans, A. Magasinski, A. S. Raman, K. Turcheniuk, S. Barlow, W. R. Dichtel, G. Yushin, S. R. Marder, *ACS Appl. Energ. Mater.* **2021**, *4*, 350–356.
[48] S. Gu, R. Hao, J. Chen, X. Chen, K. Liu, I. Hussain, G. Liu, Z. Wang, Q. Gan, H. Guo, M. Li, K. Zhang, Z. Lu, *Mater. Chem. Front.* **2022**, *6*, 2545–2550.
[49] M. Wu, Y. Zhao, H. Zhang, J. Zhu, Y. Ma, C. Li, Y. Zhang, Y. Chen, *Nano Res.* **2021**, *23*, 1–6.
[50] Y. Tong, Z. Sun, J. Wang, W. Huang, Q. Zhang, *SmartMat* **2022**,1–10.
[51] L. Zhai, G. Li, X. Yang, S. Park, D. Han, L. Mi, Y. Wang, Z. Li, S. Y. Lee, *Adv. Funct. Mater.* **2021**, 2108798.
[52] H. Zhao, H. Chen, C. Xu, Z. Li, B. Ding, H. Dou, X. Zhang, *ACS Appl. Energ. Mater.* **2021**, *4*, 11377–11385.
[53] X. Yang, C. Lin, D. Han, G. Li, C. Huang, J. Liu, X. Wu, L. Zhai, L. Mi, *J. Mater. Chem. A* **2022**, *10*, 3989–3995.
[54] Z. N. Wang, W. Z. Zheng, W. Z. Sun, L. Zhao, W. K. Yuan, *ACS Appl. Energ. Mater.* **2021**, *4*, 2808–2819.
[55] M. K. Shehab, K. S. Weeraratne, T. Huang, K. U. Lao, H. M. El-Kaderi, *ACS Appl. Mater. Interfaces* **2021**, *13*, 15083–15091.
[56] S. Vedachalam, P. Sekar, C. Nithya, N. Murugesh, R. Karvembu, *ACS Appl. Energ. Mater.* **2022**, *5*, 557–566.
[57] E. R. Wolfson, L. Schkeryantz, E. M. Moscarello, J. P. Fernandez, J. Paszek, Y. Y. Wu, C. M. Hadad, P. L. McGrier, *ACS Appl. Mater. Interfaces* **2021**, *13*, 41628–41636.
[58] a) B. Pei, D. Liu, Z. Tian, J. Huang, *ChemistrySelect* **2022**, *7*, e202200656; b) X. Chen, H. Zhang, C. Ci, W. Sun, Y. Wang, *ACS Nano* **2019**, *13*, 3600–3607.
[59] X. X. Luo, W. H. Li, H. J. Liang, H. X. Zhang, K. D. Du, X. T. Wang, X. F. Liu, J. P. Zhang, X. L. Wu, *Angew. Chem. Int. Ed.* **2022**, e202117661.
[60] a) N. Wang, Z. Guo, Z. Ni, J. Xu, X. Qiu, J. Ma, P. Wei, Y. Wang, *Angew. Chem.* **2021**, *133*, 20994–21000; *Angew. Chem. Int. Ed.* **2021**, *60*, 20826–20832; b) N. Patil, C. D. L. Cruz, D. Ciurduc, A. Mavrandonakis, J. Palma, R. Marcilla, *Adv. Energy Mater.* **2021**, *11*, 2100939.
[61] a) F. Wan, Z. Hao, S. Wang, Y. Ni, J. Zhu, Z. Tie, S. Bi, Z. Niu, J. Chen, *Adv. Mater.* **2021**, *33*, 2102701; b) Y. Fang, Y. Chen, L. Zeng, T. Yang, Q. Xu, Y. Wang, S. Zeng, Q. Qian, M. Wei, Q. Chen, *J. Colloid Interface Sci.* **2021**, *593*, 251–265.
[62] a) H. Zhang, Y. Fang, F. Yang, X. Liu, X. Lu, *Energy Environ. Sci.* **2020**, *13*, 2515–2523; b) M. Ghosh, V. Vijayakumar, M. Kurian, S. Dilwalea, S. Kurungot, *Dalton Trans.* **2021**, *50*, 4237–4243; c) M. Wu, Y. Zhang, L. Xu, C. Yang, M. Hong, M. Cui, B. C. Clifford, S. He, S. Jing, Y. Yao, L. Hu, *Matter* **2022**, *5*, 3402–3416.
[63] A. Khayum, M. Ghosh, V. Vijayakumar, A. Halder, M. Nurhuda, S. Kumar, M. Addicoat, S. Kurungot, R. Banerjee, *Chem. Sci.* **2019**, *10*, 8889.
[64] W. Wang, V. S. Kale, Z. Cao, S. Kandambeth, W. Zhang, J. Ming, P. T. Parvatkar, E. A. Hamad, O. Shekhah, L. Cavallo, M. Eddaoudi, H. N. Alshareef, *ACS Energy Lett.* **2020**, *5*, 2256–2264.
[65] W. X. Wang, V. S. Kale, Z. Cao, Y. Lei, S. Kandambeth, G. D. Zou, Y. P. Zhu, E. Abouhamad, O. Shekhah, L. Cavallo, M. Eddaoudi, H. N. Alshareef, *Adv. Mater.* **2021**, 2103617.
[66] M. H. Yu, N. Chandrasekhar, R. K. M. Raghupathy, K. H. Ly, H. Z. Zhang, E. Dmitrieva, C. L. Liang, X. L. Lu, T. D. Kühne, H. Mirhosseini, I. M. Weidinger, X. L. Feng, *J. Am. Chem. Soc.* **2020**, *142*, 19570–19578.
[67] S. B. Zheng, D. J. Shi, D. Yan, Q. R. Wang, T. J. Sun, T. Ma, L. Li, D. He, Z. L. Tao, J. Chen, *Angew. Chem. Int. Ed.* **2022**, *61*, e202117511.
[68] D. Ma, H. Zhao, F. Cao, H. Zhao, J. Li, L. Wang, K. Liu, *Chem. Sci.* **2022**, *13*, 2385.
[69] H. L. Cui, T. R. Wang, Z. D. Huang, G. J. Liang, Z. Chen, A. Chen, D. H. Wang, Q. Yang, H. Hong, J. Fan, C. Y. Zhi, *Angew. Chem.* **2022**, e202203453.
[70] R. M. Sun, S. Y. Hou, C. Luo, X. Ji, L. N. Wang, L. Q. Mai, C. S. Wang, *Nano Lett.* **2020**, *20*, 3880–3888.
[71] S. Borhani, M. Moradi, M. Pooriraj, B. Chameh, *Surf. Interfaces* **2021**, *26*, 101313.
[72] Q. F. Zhang, H. P. Wei, L. L. Wang, J. Wang, L. Fan, H. B. Ding, J. Y. Lei, X. Z. Yu, B. G. Lu, *ACS Appl. Mater. Interfaces* **2019**, *11*, 44352–44359.
[73] H. Y. Lu, F. Y. Ning, R. Jin, C. Teng, Y. Wang, K. Xi, D. S. Zhou, G. Xue, *ChemSusChem* **2020**, *13*, 3447–3454.
[74] Q. H. Geng, H. C. Wang, J. L. Wang, J. Hong, W. W. Sun, Y. Wu, Y. Wang, *Small Methods* **2022**, *6*, 2200314.
[75] Y. Q. Cai, Z. T. Gong, Q. Rong, J. M. Liu, L. F. Yao, F. X. Cheng, J. J. Liu, S. B. Xia, H. Guo, *Appl. Surf. Sci.* **2022**, *594*, 153481.
[76] S. W. Li, Y. Z. Liu, L. Dai, S. Li, B. Wang, J. Xie, P. F. Li, *Energy Storage Mater.* **2022**, *48*, 439–446.
[77] a) A. Venkatesha, R. Gomes, A. S. Nair, S. Mukherjee, B. Bagchi, A. J. Bhattacharyya, *ACS Sustainable Chem. Eng.* **2022**, *10*, 6205–6216; b) X. L. Liu, Y. C. Jin, H. L. Wang, X. Y. Yang, P. P. Zhang, K. Wang, J. Z. Jiang, *Adv. Mater.* **2022**, 2203605; c) M. Y. Yao, C. F. Guo, Q. H. Geng, Y. F. Zhang, X. Zhao, Y. Wang, *Ind. Eng. Chem. Res.* **2022**, *61*, 7480–7488; d) G. Wang, N. Chandrasekhar, B. P. Biswal, D. Becker, S. Paasch, E. Brunner, M. Addicoat, M. H. Yu, R. Berger, X. L. Feng, *Adv. Mater.* **2019**, 1901478.
[78] J. J. Zhao, M. M. Zhou, J. Chen, L. H. Tao, Q. Zhang, Z. F. Li, S. W. Zhong, H. K. Fu, H. Wang, L. J. Wu, *Chem. Eng. J.* **2021**, *425*, 131630.
[79] S. B. Xia, Y. Q. Cai, L. F. Yao, J. Y. Shi, F. X. Cheng, J. J. Liu, Z. J. He, J. C. Zheng, *Energy Storage Mater.* **2022**, *50*, 225–233.
[80] G. Zhao, Y. Sun, Y. Yang, C. Zhang, Q. An, H. Guo, *EcoMat.* **2022**, e212221.
[81] M. M. Wu, Y. Zhao, R. Q. Zhao, J. Zhu, J. Liu, Y. M. Zhang, C. X. Li, Y. F. Ma, H. T. Zhang, Y. S. Chen, *Adv. Funct. Mater.* **2022**, *32*, 2107703.
[82] G. F. Zhao, H. Li, Z. H. Gao, L. F. Xu, Z. Y. Mei, S. Cai, T. T. Liu, X. F. Yang, H. Guo, X. L. Sun, *Adv. Funct. Mater.* **2021**, *31*, 2101019.
[83] R. Zhou, Y. Huang, Z. H. Li, S. Kang, X. M. Wang, S. Y. Liu, *Energy Storage Mater.* **2021**, *40*, 124–138.
[84] H. Z. Zhao, D. R. Luo, H. Xu, W. J. He, B. Ding, H. Dou, X. G. Zhang, *J. Mater. Sci.* **2022**, *57*, 9980–9991.
[85] C. G. Wu, M. J. Hu, X. R. Yan, G. C. Shan, J. Z. Liu, J. Yang, *Energy Storage Mater.* **2021**, *36*, 347–354.
[86] J. Duan, W. T. Wang, D. G. Zou, J. Liu, N. Li, J. Y. Weng, L. P. Xu, Y. Guan, Y. J. Zhang, P. F. Zhou, *ACS Appl. Mater. Interfaces* **2022**, *14*, 31234–31244.
[87] L. Zhao, L. Zheng, X. P. Li, H. Wang, L. P. Lv, S. Q. Chen, W. W. Sun, Y. Wang, *ACS Appl. Mater. Interfaces* **2021**, *13*, 48913–48922.
[88] Z. R. Lin, L. Lin, J. Q. Zhu, W. L. Wu, X. P. Yang, X. Q. Sun, *ACS Appl. Mater. Interfaces* **2022**, *14*, 38689–38695.
[89] Z. Z. Yang, H. Chen, S. Wang, W. Guo, T. Wang, X. Suo, De-en Jiang, X. Zhu, I. Popovs, S. Dai, *J. Am. Chem. Soc.* **2020**, *142*, 6856–6860.

Manuscript received: December 14, 2022
Revised manuscript received: January 15, 2023
Accepted manuscript online: January 23, 2023
Version of record online: February 8, 2023